Measurements at the DL0SHF 24 GHz Antenna

Joachim Köppen, DF3GJ
Inst.Theoret.Physik u.Astrophysik, Univ. Kiel
August 2015

Pointing Correction

Until 2014, this antenna had successfully withstood all attempts to make it track the Sun or the Moon either with simple correction tables or the Bodenschief correction model. Let us summarize an otherwise longish history: measurements of solar positions by DK7LJ during one day in September 2014 revealed that the original Bodenschief model is not capable to correct the errors in azimuth:

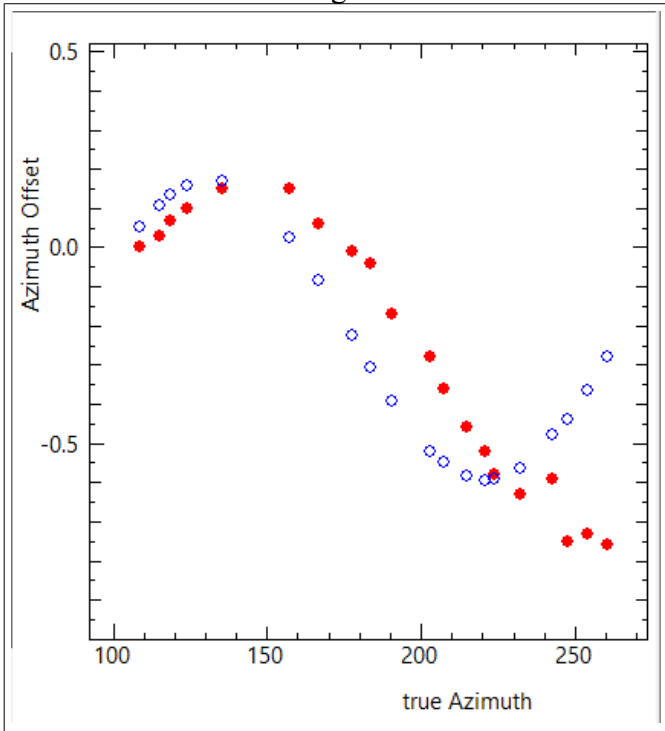

Fig. 1a *Comparison of observed azimuth offsets (red dots) with predictions (blue circles) from the Bodenschief model fitted to these data.*

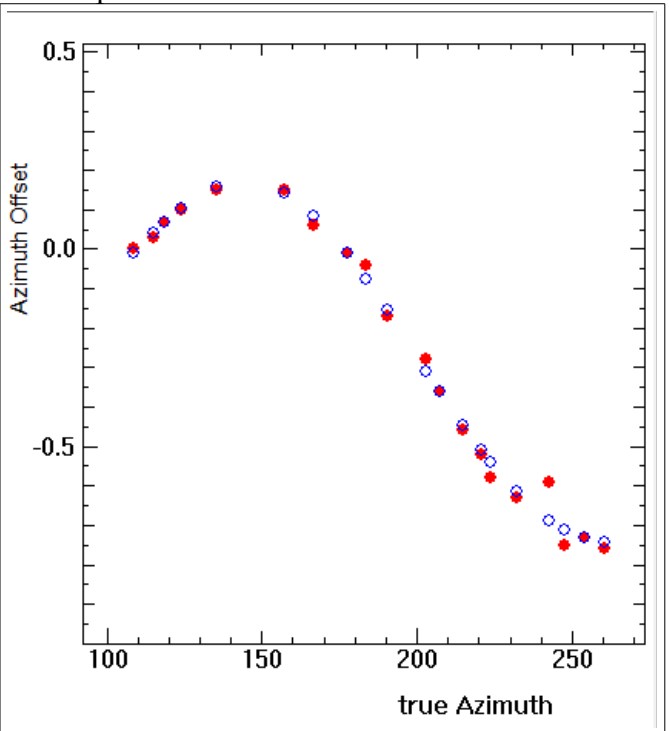

Fig. 1b *As Fig1a, but for the P-model.*

The Bodenschief model fit to the data (Fig.1a) gives an entirely unsatisfactory residual r.m.s. error of 0.2°. In particular, it presents a very poor match of the azimuth dependence of the azimuth offsets. Interpretation with a P-model results in a much better r.m.s. residual 0.03°, close to the tracking accuracy, and gives a nearly perfect fit (Fig.1b). It is found that inclusion of the P2 and P3 terms is crucial, which model the collimation error and the elevation axis tilt, respectively.

In spring 2015 the gearbox and the motors underwent a thorough refurbishment. Upon this, measurements of position errors of the Sun and the Moon were taken. Instead of simply trying to reach the maximum signal, the improved method of bracketing the position of the maximum is used, giving

an accuracy of 0.01°. While a fit with a Q18 model gives an excellent r.m.s. error of 0.02° and the scatter during each day or night is of the order of 0.01°, it is noticed that the data taken at earlier times are incompatible to those taken a few days later (Fig.2). Changes of the basic settings of the motor drives are eventually excluded, and a systematic trend is found in that the errors become more negative in time. This means that the position of a celestial object seems to slip towards the West.

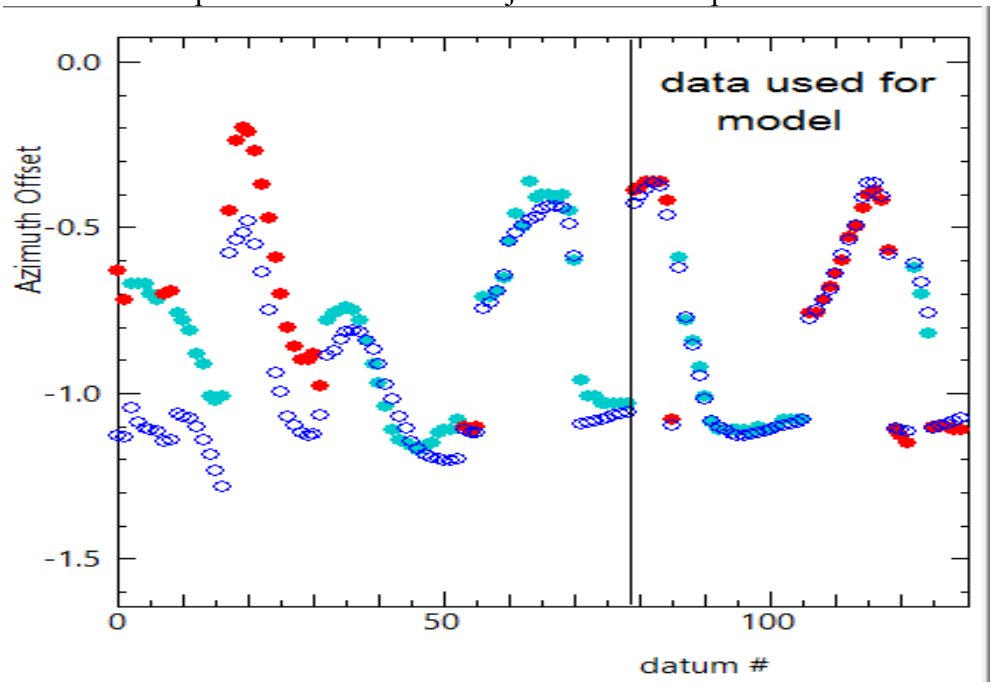

Fig. 2 *Evolution of the azimuth offsets in comparison to predictions from a Q18 model fitted to the data of Sun (red dots) and Moon (blue-green dots) from the last three days.*

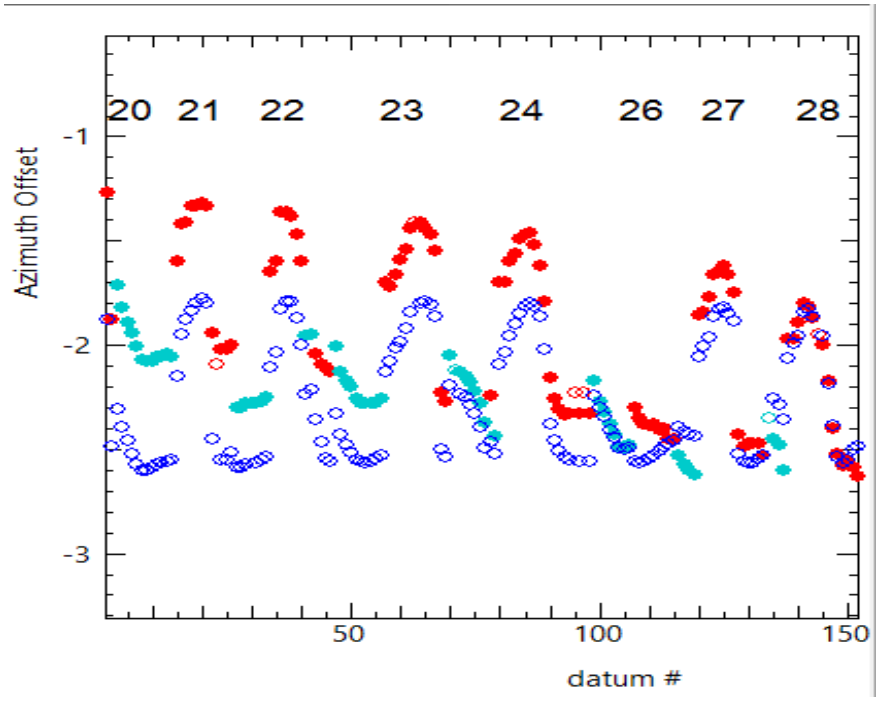

Fig. 3 *Evolution of the azimuth offsets, compared to the Q24 model that is matched to the last day's data (with r.m.s. deviation of 0.007°). The numbers indicate the days of July 2015.*

More systematic measurements taken in July 2015 (Fig. 3) prove the systematic slipping of the azimuth offsets. There is not the slightest deviation in elevation offsets from the model predictions. Obviously, this is a mechanical slippage of the azimuth axis. Inspection confirms this findings and the mechanics is improved.

Subsequent measurements in August 2015 confirm the improved stability. There still remains a very slight slippage in azimuth – of perhaps 0.02° – which is hardly detectable in the signal level. However, it is noticed that the first measurement after a wide slew across the sky from West to East always gives an azimuth offset rather different from the model prediction (Fig.4), while the following measurements agree well with the predictions. A long slew from East to West does not show any such effect.

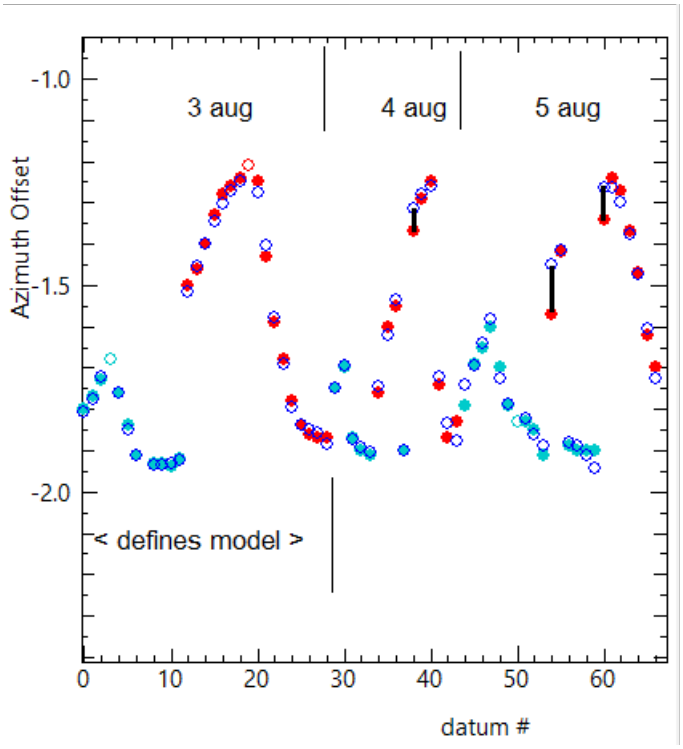

Fig. 4 *Evolution of the azimuth offsets, compared to the predictions of the Q24 model fit to the first day's data. The black bars mark the large offsets found at the first measurement after a wide slew across the sky from West to East.*

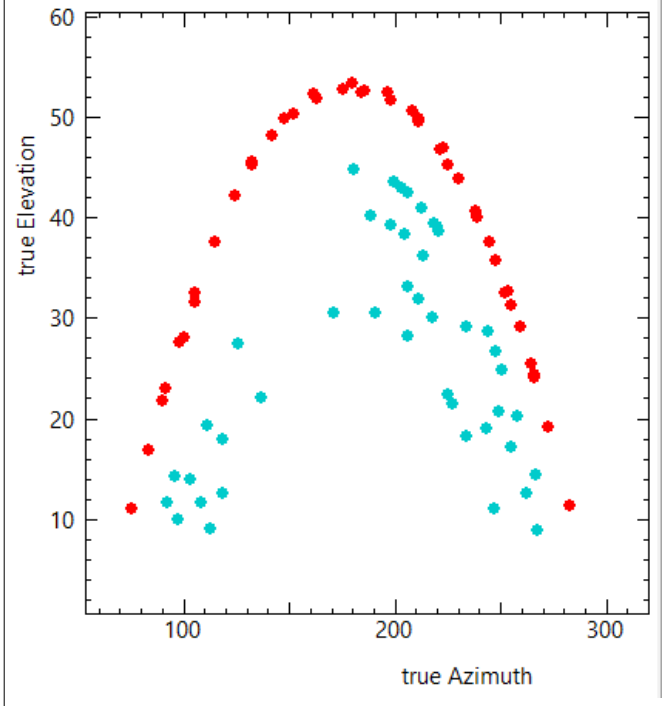

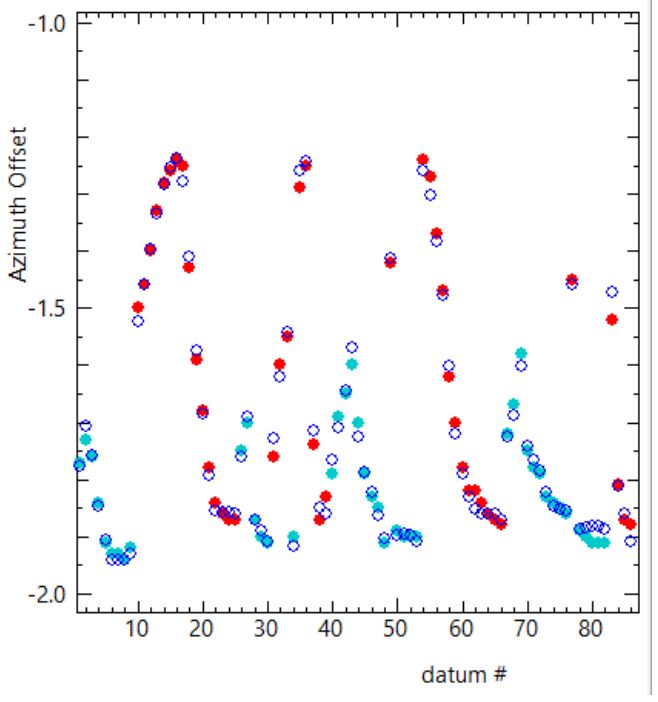

Fig. 5a *The sky coverage of the recommended data set from 3..6 August 2015*

Fig. 5b *The adopted Q24 model fits all data with an r.m.s. residual of 0.015°*

As the remaining issues in azimuth have very little effect on the signal strength, one may use the data from August 2015 to establish an acceptable pointing correction model (Figs. 5a, b).

Antenna Pattern

The antenna pattern is measured by drift scans of the Sun near noon so that the apparent motion of the Sun is only in horizontal direction. One complete scan takes about 1 hour. There is a slight variation of the sky foreground (typically 0.03 dB) by passing clouds and (possibly) thermal inhomogeneities. The time evolution of the sky emission is manually matched by a piece-wise linear function. This function is subtracted (in linear power) from the scan data to yield the antenna pattern. Several successive scans are taken from which the best is selected, but the others are useful to confirm the side lobe pattern.

For the 24 GHz antenna two feeds were tested: (a) the usually used horn (**more details** …?) and (b) the open end of the waveguide.

Let us first take a look at the main lobe, presented as the data appears in the normal plot of received power level against time.

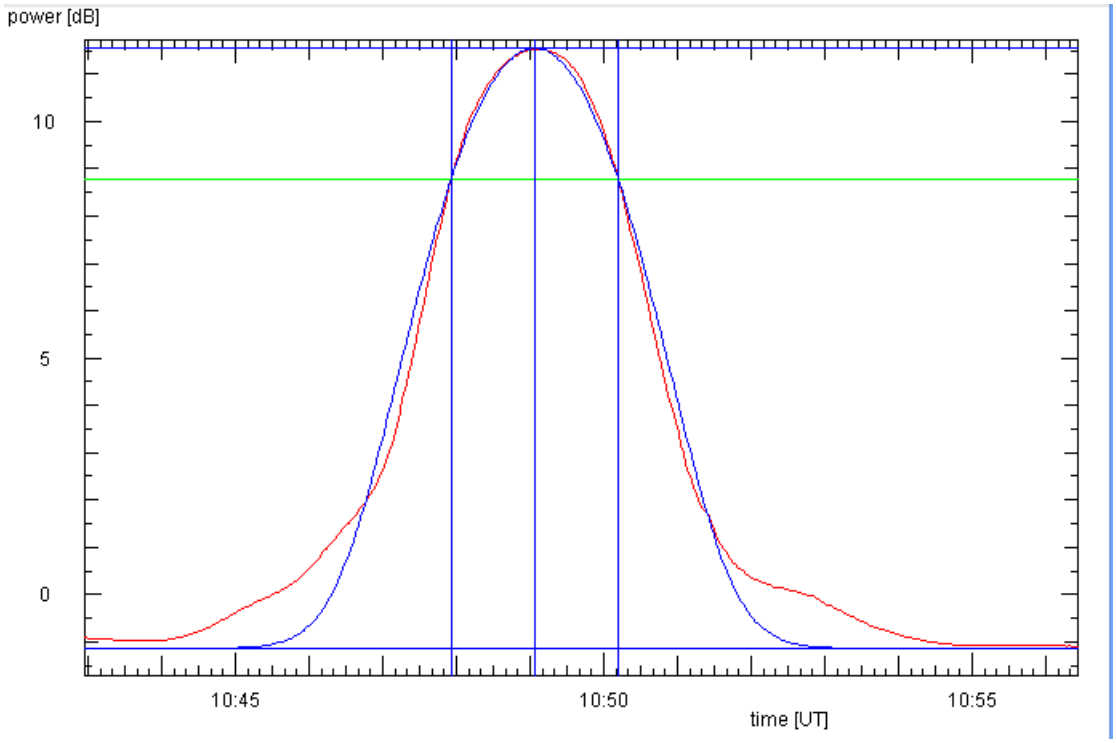

Fig. 6a *The main lobe of the pattern with the horn feed (red curve). The fit with a Gaussian function (blue curve) yields a FWHM of 0.59° (after correction for solar declination). The horizontal blue lines mark the levels of the maximum and of the assumed sky foreground. The green horizontal line indicates the level of half maximum power, while the vertical blue lines indicate the times of the half-power points.*

Figure 6a shows that the main lobe – with the horn feed – is well reproduced with a Gaussian function, and that side lobes become apparent 10 dB below the maximum. Since the Sun's angular diameter of 0.52° is larger than the theoretical width of the main lobe, this pattern is but the true pattern folded with the intensity profile of the Sun (see below), and all structures are strongly smoothed.

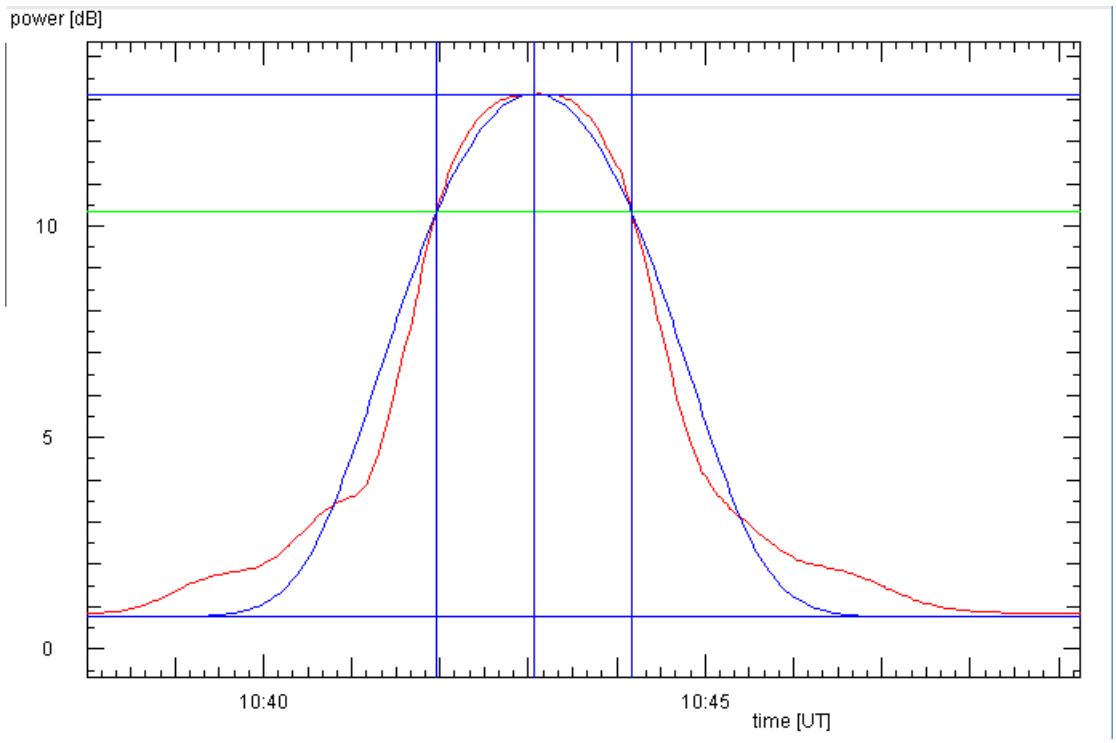

Fig. 6b *Same as Fig.6a, but for the open waveguide feed. The FWHM of the Gaussian is 0.57°.*

The main lobe – with the open waveguide feed – has some top flattening in the centre, is a little bit stronger on the Eastern side, and has flanks which are steeper than a Gaussian function. Like before, side lobes become apparent near 10 dB below the maximum. Apart from minor differences, the pattern is almost identical to that with the horn feed.

Plots of the difference of observed power and the sky foreground power reveal the detailed structure of the side lobes:

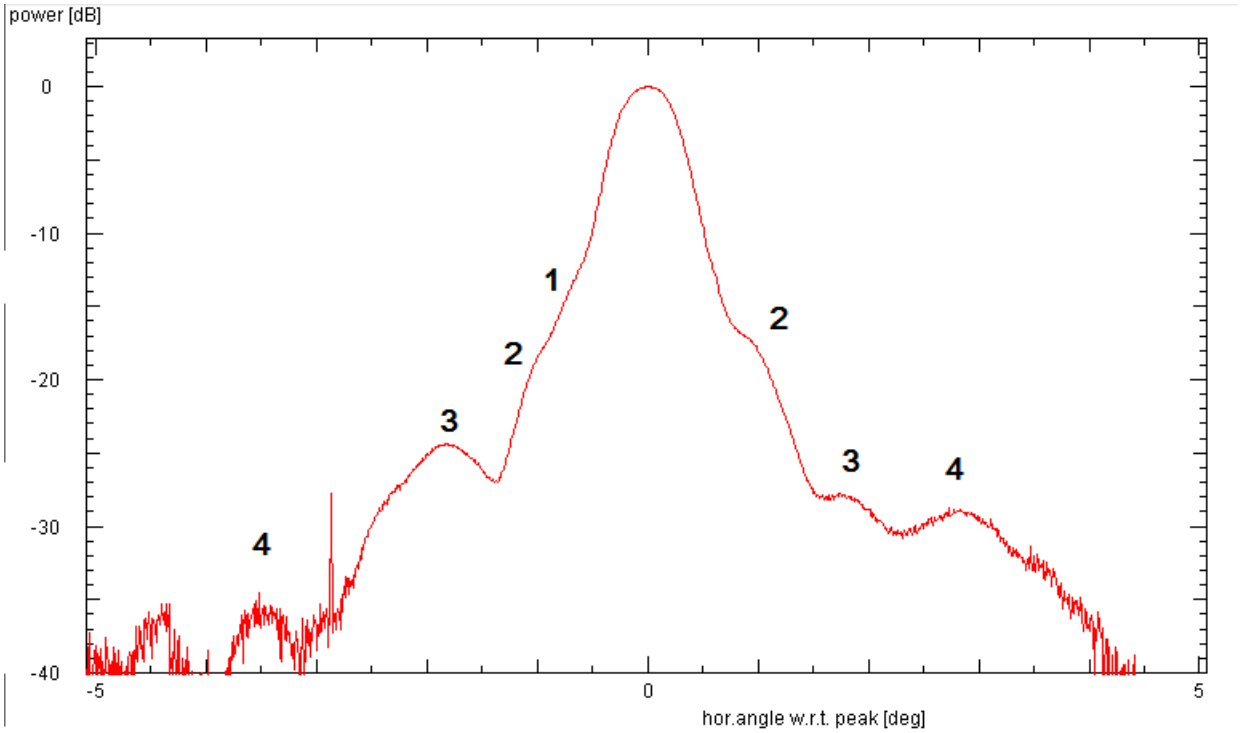

Fig. 7a *Observed antenna pattern with the horn feed. Note that the right hand side is the Eastern part of the pattern. The numbers label the side lobes.*

Figure 7a displays the pattern with the normal horn feed. One notes that

- the main beam is nicely symmetric
- first and second side lobes appear in the flank of the main lobe
- first side lobe is almost absent on the Eastern side
- the second side lobe is more prominent on the Eastern side, while the third side lobe is stronger on the Western side.
- side lobes beyond the 2nd one are down by about 20 dB, any presence of a 5th side lobe is masked by variations of the sky foreground which correspond to 35..40 dB below the main lobe.

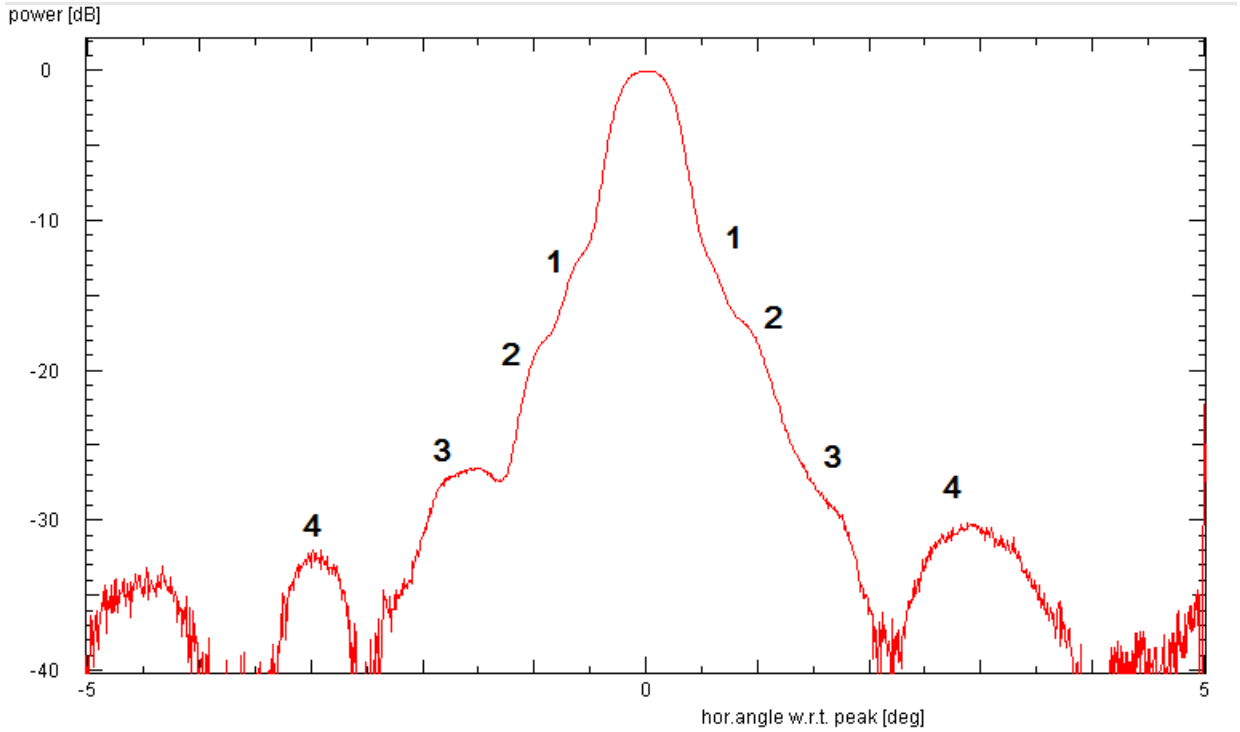

Fig. 7b *Observed pattern with the open waveguide as a feed. The numbers label the side lobes.*

The pattern obtained with bare open waveguide (Fig.6b) closely resembles the other one. There are a few minor differences:

- the main lobe looks broader
- first side lobe is more clearly visible on both sides
- 2nd side lobe is more prominent on the Eastern side, while the 3rd lobe is stronger on the West side (as with the horn). However, the West 3rd lobe is a few dB lower than with the horn feed.
- the fourth side lobe is stronger than with the horn feed

The interpretation of the observed patterns needs to take into account the finite size of the solar disk. Since the emission at 24 GHz comes from the chromosphere, one may represent the Sun by a uniformly illuminated disk of 0.52° diameter. Rather than trying to deconvolve the observed pattern, it is best to convolve theoretical patterns with the solar disk image to create the observable pattern. This is done using the theoretical pattern from a uniformly illuminated circular aperture of the specified diameter.

The most important features seen in the observed data are the FWHM of the main lobe and the number of side lobes within 3° of the centre, which is four. The modeling tries to reproduced these facts. Also, one may use the position and the depth of the prominent null between 2nd and 3rd Western side lobes.

Antenna diametre [m]	HPBW [°]	FWHM (with Sun) [°]
1	0.741	0.786
1.2	0.611	0.672
1.3	0.568	0.637
1.4	0.526	0.600

1.5	0.488	0.573
1.6	0.460	0.546
2	0.370	0.499
3	0.243	0.497
4	0.184	0.510

The above table shows that if one wants to reproduce the measured FWHM = 0.59°, an effective antenna diameter of 1.4 m is required, whose pattern is shown in Fig. 8a.

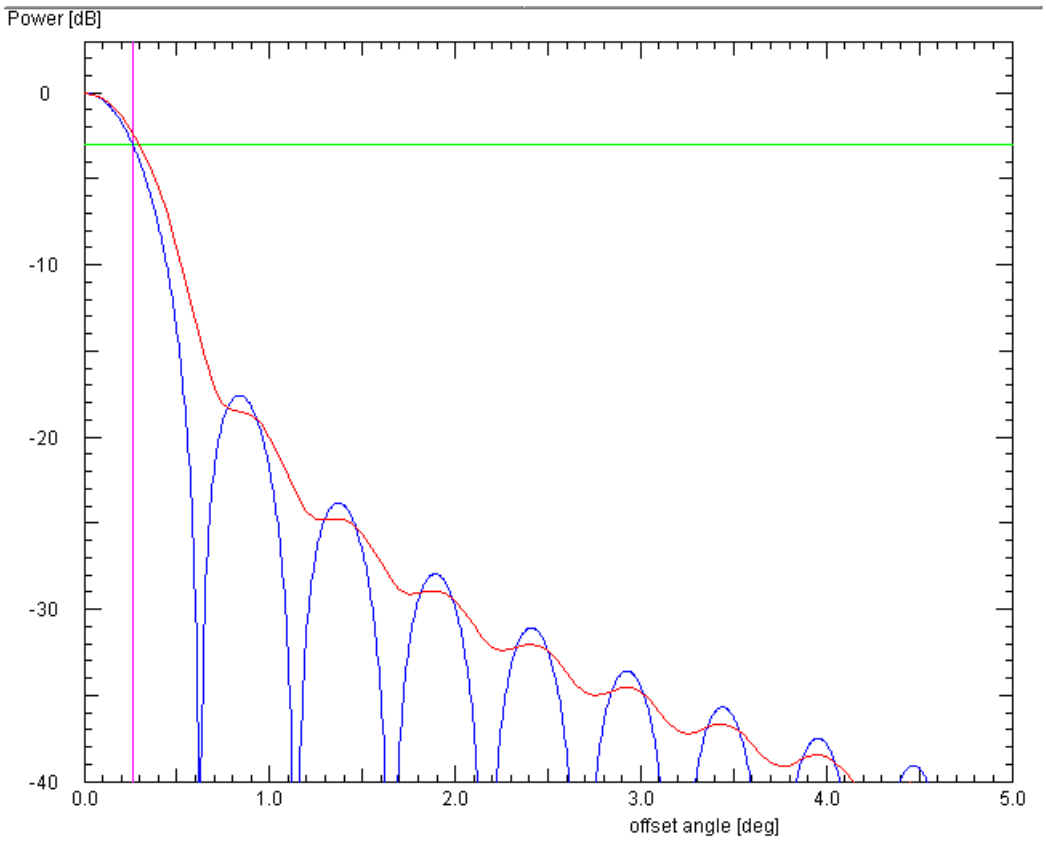

Fig. 8a *The theoretical pattern (blue curve) of a uniformly illuminated 1.4 m diameter circular aperture antenna convolved with a uniformly bright circular solar disk of 0.52° angular diameter.*

However, predicted side lobes are spaced too closely: There are 5 side lobes within 3° of the beam centre. If one wanted only 4 side lobes, the antenna's diameter should be 1.2 m (Fig. 8b). This latter model would also account better for the positions of the nulls (or minima).

This modeling should not be taken too far: the real antenna is not a uniformly illuminated dish, and the illumination characteristics strongly influences the side lobe pattern. For instance, one notes that the first side lobe is 20 dB down from the maximum, whereas in the observed pattern it is present already at –10 dB (cf. Fig.7b). On the other hand, the side lobes near 3° are at 35 dB below the maximum, which is consistent with the measurements. Thus, the truth is nearby!

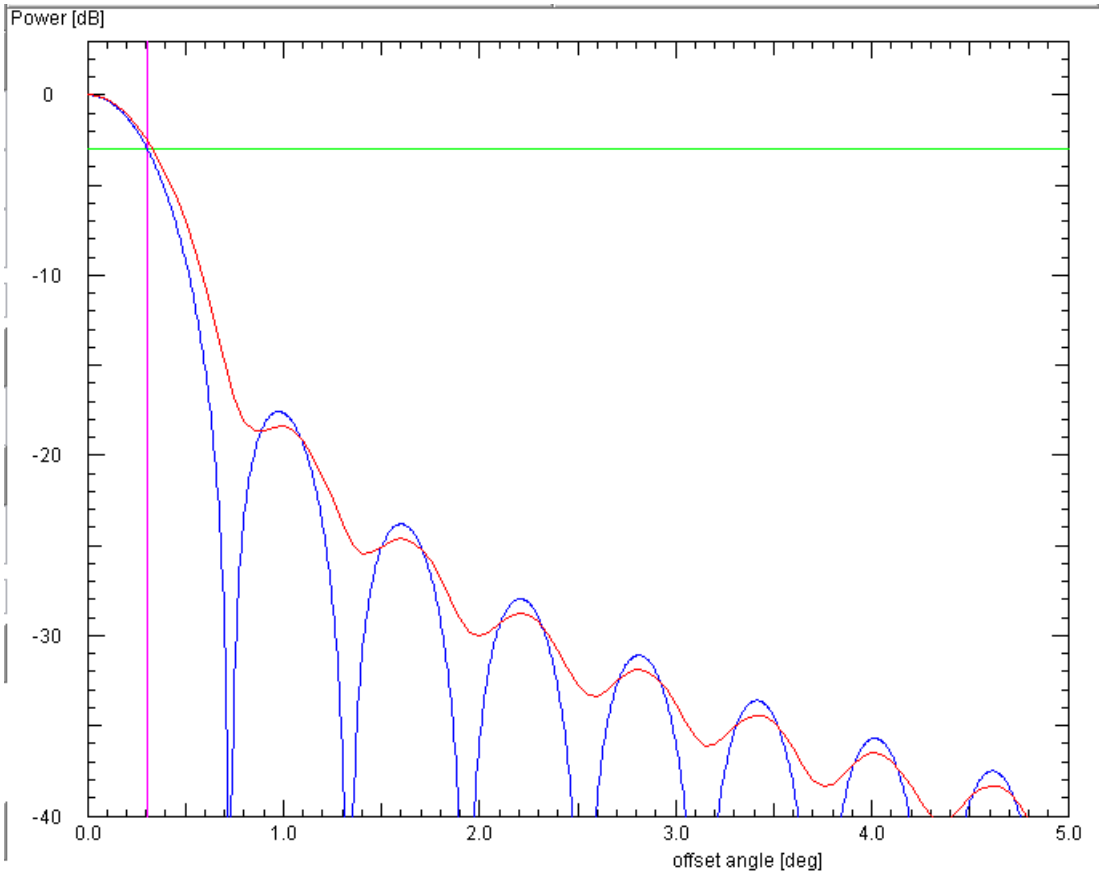

Fig. 8b *Same as Fig.8a, but for a dish diameter of 1.2 m.*

This implies that the 24 GHz mirror is illuminated only in its central portion. Since it is a rather deep dish (ratio of focal length to diameter f/D = 0.35), it requires a feed with a very wide radiation pattern, which the present feeds cannot supply. Thus, with an outer diameter of 4.3 m, the (aperture) efficiency is only 10 percent!

The gain of the antenna is about 49.6 dBi, and its true HPBW is about 0.6°, about 3 times the value expected for the entire dish.

What would be, if the full dish would be uniformly illuminated? This is shown in Fig.8c for a diameter of 4 m: the solar disk would be resolved, and the first 4 side lobes would be within 1° of the centre. The observed pattern would be rather smooth, showing only hints of the side lobes and no prominent nulls.

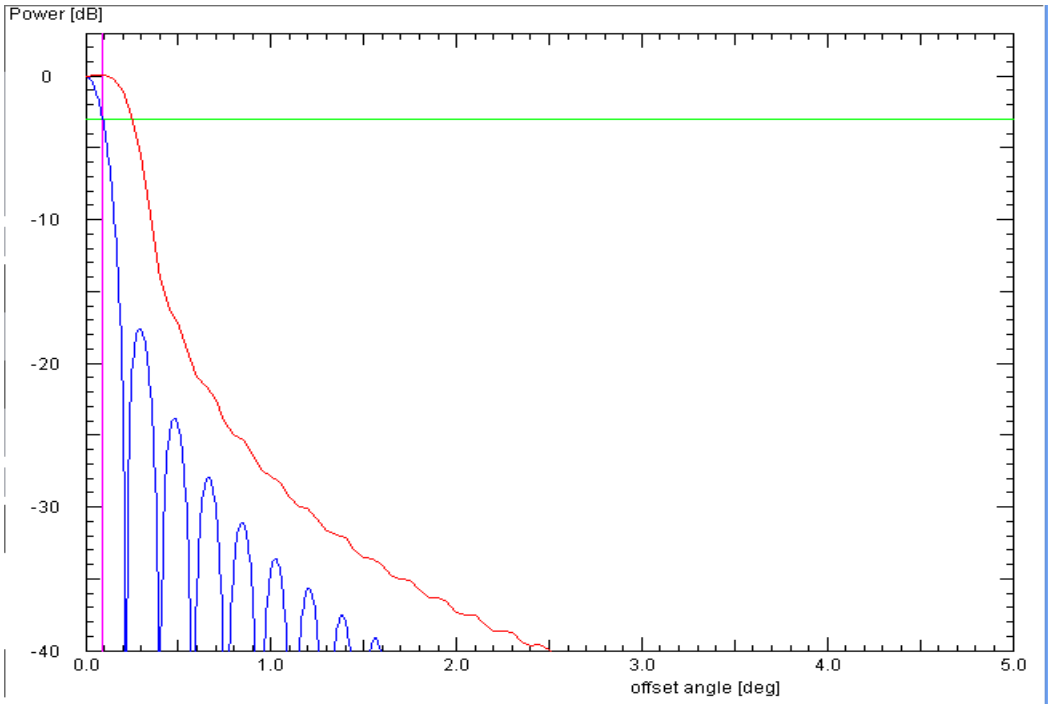

Fig. 8c *Same as Fig.8a, but for a dish diameter of 4 m.*

The small effective diametre is corroborated by the absence of spill-over, as is evident by the absence of noise increasing towards the zenith (Fig. 9).

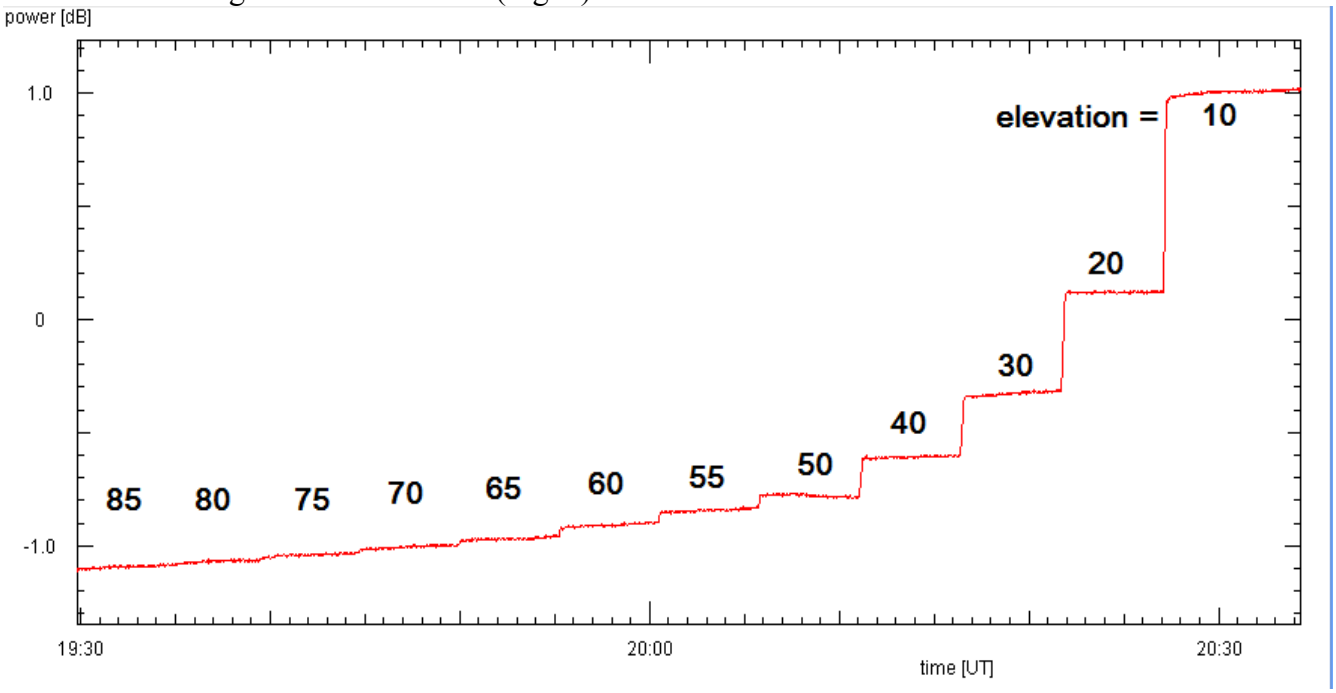

Fig. 9 *The noise level by the sky foreground does not show any increase toward the zenith.*

Sky Profile with Absorption: 'Theory'

The analysis of the sky profile (as explained in the Technical Note *Measurements with the DL0SHF 1 GHz Radio Telescope*) can be generalized by taking into account the absorption of the atmosphere in the following way. In order to keep explanations straight and simple and to avoid unnecessary mathematical complexities in the formulae, we shall assume that the column of air has constant temperature and density.

Consider a column of air with given length L and with a certain constant absorption coefficient κ, which describes how much a unit length of air absorbs. The intensity (or power, but here expressed in antenna temperature T) of a radio (or light) wave passing through this medium is reduced following this law

$$T = T_0 \exp(-\kappa * L) = T_0 \exp(-\tau)$$

where T_0 is the antenna temperature of the incident wave. Thus, a long column of low absorption air has the same effect as a short column of highly absorbing material. The essential quantity is the product of geometrical thickness of an object and its absorption coefficient which is called the object's **optical thickness** $\tau = \kappa * L$.

This column of air also emits thermal radiation, the amount of which depends on the air temperature, absorption coefficient, and the length of the column: The antenna temperature of this radiation is

$$T = T_{AIR} (1 - \exp(-\tau))$$

where T_{AIR} is the physical temperature of the air.

Taking both effects together, the antenna temperature of a celestial source with antenna temperature T_0 seen through a column of absorbing and emitting air with temperature T_{AIR} is

$$T = T_0 \exp(-\tau) + T_{AIR} (1 - \exp(-\tau))$$

This is the general case, which we shall need to refer to again.

The sky profile is nothing but the measurement of the emission of the atmosphere at various elevations. Since in a plane-parallel atmosphere the length L of the column depends on the elevation ε by

$$L(\varepsilon) = L(90°) / \sin(\varepsilon)$$

it is convenient to use the **air mass** $A = 1/\sin(\varepsilon)$ instead of the elevation. Note that at the zenith A = 1.0. Thus

$$L(A) = L(1.0) * A$$

This gives for the sky profile

$$T(A) = T_{AIR} (1 - \exp(-\tau(A)) = T_{AIR} (1 - \exp(-\tau(1)*A))$$

Here exp(τ(1.0)) is the atmospheric attenuation at the zenith, which will be some constant describing the present state of the atmosphere.
While this formula looks complicated, it contains the formula used before, i.e. when the absorption was not taken into account: For small values of x one has approximately exp(-x) ≈ 1 – x, so that for a transparent atmosphere the formula becomes

$$T(A) = T_{AIR}\,(1 - \exp(-\tau(1)*A)) \approx T_{AIR}\,(1 - (1-\tau(1)*A)) = T_{AIR} * \tau(1) * A = T_{zenith} * A$$

which is the previously used formula.

The essential feature of a sky profile in an atmosphere with appreciable absorption is that the relationship between noise power and air mass is no longer the linear (straight line) function of the transparent atmosphere. Instead the sky profiles show a clear curvature, as shown in Fig 10b in comparison with 1.3 GHz observations (Fig. 10a). In order to measure the curvature more reliably, the 24 GHz profile is done with a finer spacing in elevations between 10 and 30°.

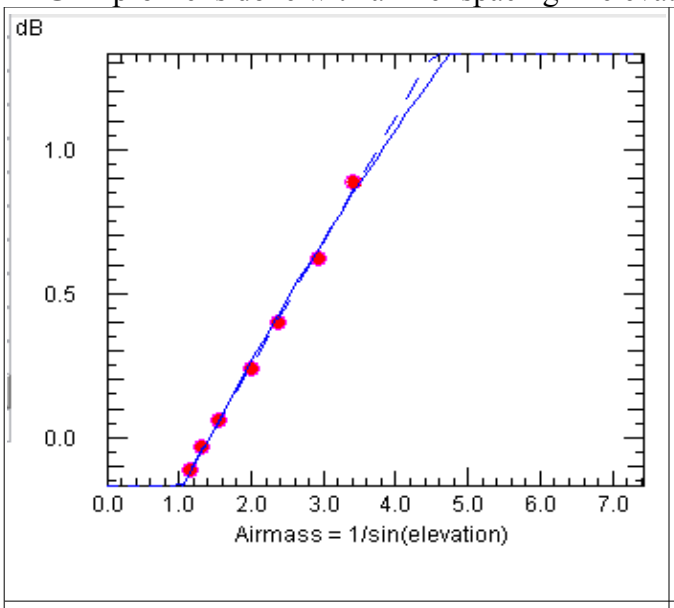

Fig. 10a *A sky profile on 1.3 GHz*

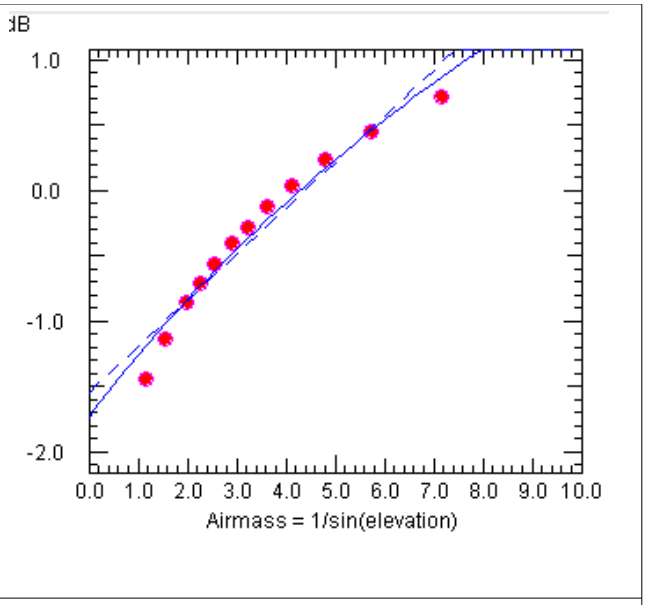

Fig. 10b *Sky profile on 24 GHz*

Interpretation

Since the raw measurements are in terms of the received power p, and not yet in antenna temperature, the measurement of the power p_{cal} from a flux calibrator (with temperature T_{cal}) is also necessary to determine the factor of proportionality a. Thus one needs to solve

$$p_{cal} = a * (T_{sys} + T_{cal})$$
$$p(A) = a * (T_{sys} + T(A) + T_{CMB})$$

Since $a = p_{cal} / (T_{sys} + T_{cal})$, one needs to interpret

$$p(A) = p_{cal} * (T_{sys} + T(A) + T_{CMB}) / (T_{sys} + T_{cal})$$

from which one also works out the system temperature T_{sys} as explained in the Technical Note *Measurements with the DL0SHF 1 GHz Radio Telescope* and on the DL0SHF website page *Radioastronomy/Earth atmosphere*.

While previously one had to fit the data with a straight line via

$$T(A) = T_{zenith} * A$$

one is now faced with the task of matching the data not only with the more complex formula

$$T(A) = T_{AIR} (1 - \exp(-\tau(1)*A))$$

but also to determine two parameters: T_{AIR} and $\tau(1)$ which are the temperature of the air and the optical thickness of the atmosphere at the zenith. The latter may also be more conveniently expressed in decibels per air mass:

$$Z = 10 * \log_{10}(\exp(\tau(1))) = 4.343 * \tau(1) = 4.343 * \kappa * L(1)$$

Furthermore, there is the relation

$$T_{AIR} * \tau(1) = T_{zenith}$$

Therefore, one may choose to determine any two of the parameters: T_{AIR}, T_{zenith}, or Z.

There are two possibilities: The first one is to simply guess values for T_{sys} , T_{AIR} and Z, plot the resulting curve of T(A) versus A and compare with the data. Then one modifies the guess values until all measured points lie on the curve. This is done in Fig.11

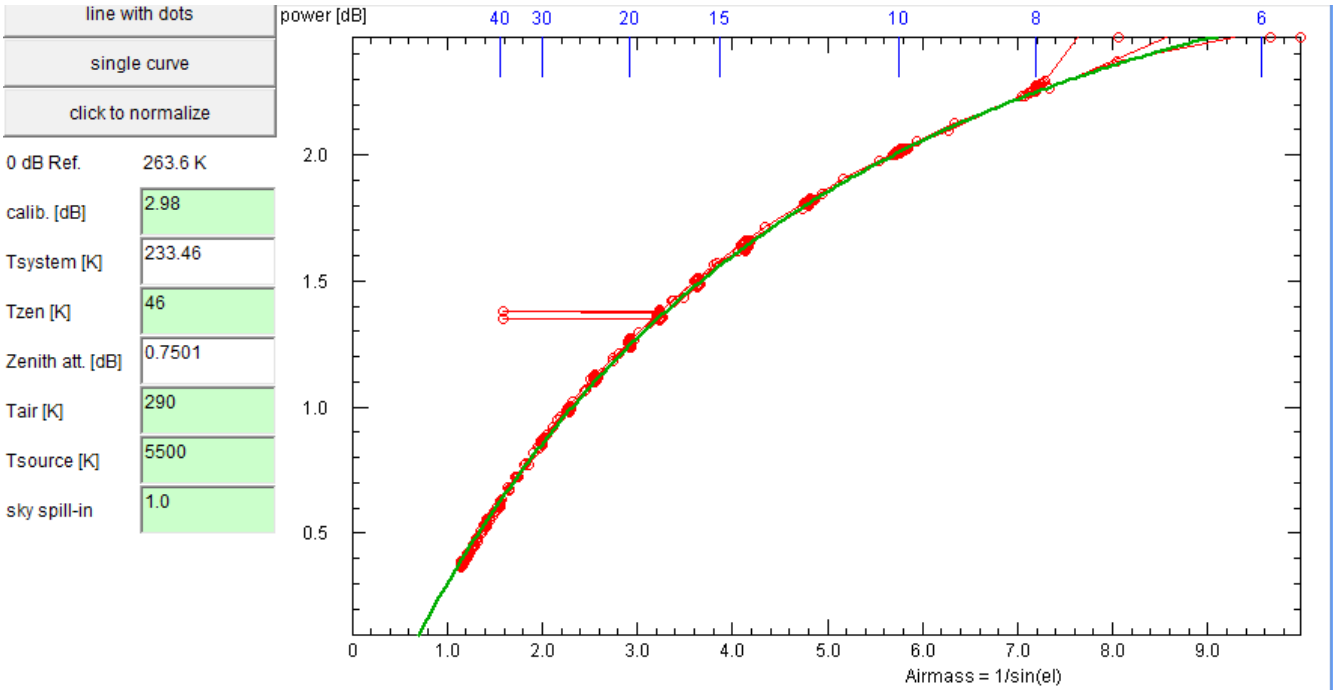

Fig. 11 *Interpretation of measurements of the sky background (red dots) as a function of elevation (top scale) or air mass (bottom scale) with a model (green curve) whose parameters are given on the panel at left. Green fields are the user-specified parameters, but Tsource and sky spill-in have no relevance here. White fields are parameters computed by the program.*

This actually is less complicated than it seems: since in the transparent atmosphere one has

$$T_{zenith} = T_{AIR} * \tau(1) = T_{AIR} * Z/4.343$$

increasing T_{AIR} or Z by the same amount gives the zenith temperature. Thus it is more practical to assume a reasonable air temperature (250 or 290 K) and then search for the best values of the zenith temperature T_{zenith}. Furthermore, after a few measurements the value for the system temperature will be well known, and can be assumed to be independent of the sky situation.

By matching the sky measurements, one may not need to make a flux calibration measurement. Instead, the factor *a* which scales antenna temperatures to power values can be derived from making the curve always passing through one of the measured points, which scales the model to the data. Thus, one executes a flux calibration by matching the exact shape of the observed relation between power and air mass, viz. elevation. However, one finds that the system temperature may not be well constrained. With the present set of data, assumption of any system temperature between 150 and 250 K leads to satisfactory results.

The reason is that the curvature of the power-airmass relation is influenced by all three free parameters, i.e. system temperature, zenith temperature, and air temperature, in a similar way, as shown in Fig.12. Therefore, an overestimated zenith temperature can be compensated by raising the system temperature or reducing the air temperature.

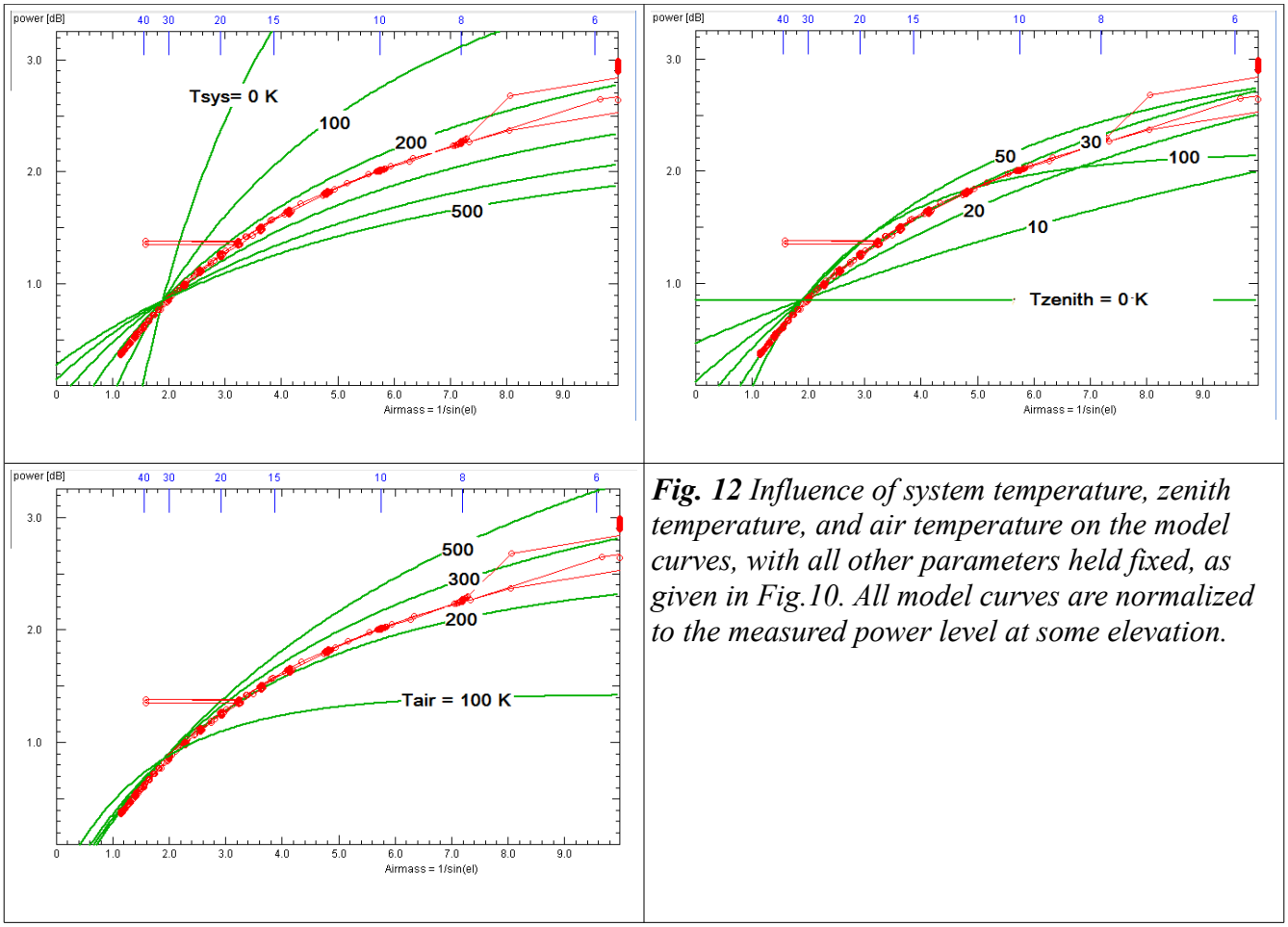

Fig. 12 *Influence of system temperature, zenith temperature, and air temperature on the model curves, with all other parameters held fixed, as given in Fig.10. All model curves are normalized to the measured power level at some elevation.*

Inclusion of the measurement of the flux calibrator reduces this uncertainty on the system temperature, because of the additional information. Therefore this is the recommended procedure, which is already used in Fig.11.

The second approach does not try to fit T(A) but instead it deals with the modified quantity

$$T(A)*A/(1 - \exp(-\tau(1)*A)) = T_{AIR} * A$$

given a guess value for $Z = 4.343*\tau(1)$. Thus again, one only needs to fit a straight line with respect to A. This can be done by linear regression. Then one searches for that value of Z whose fit gives the lowest r.m.s. deviation r, or the highest value for 1/r. Thus the method is easily formulated as an automatic procedure.

This is shown in Fig.13. This method gives the same results as the first one. But it has the advantages that the fitting is done automatically by linear regression and by a simple scan in X, and one does not need to think about starting values or pay attention of the behaviour of the model curve on the parameters, as in the first method.

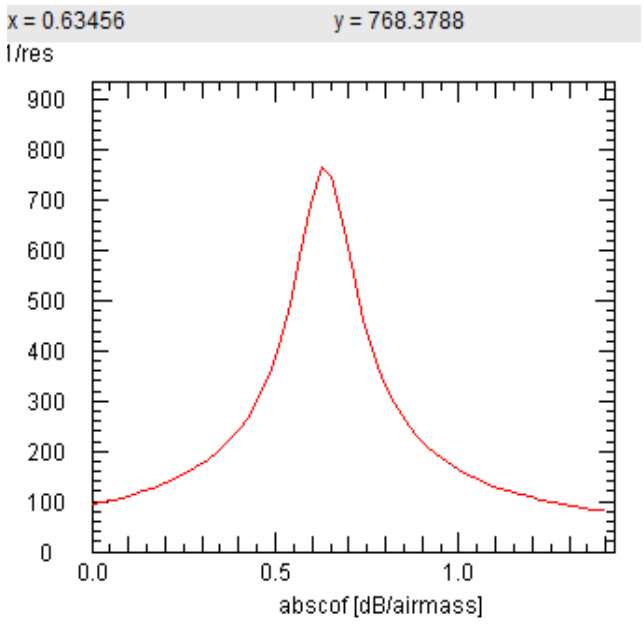

Fig. 13a *Interpretation of a sky profile: At the value of Z = 0.64 dB/airmass for the zenith attenuation the r.m.s. deviation res is minimal.*

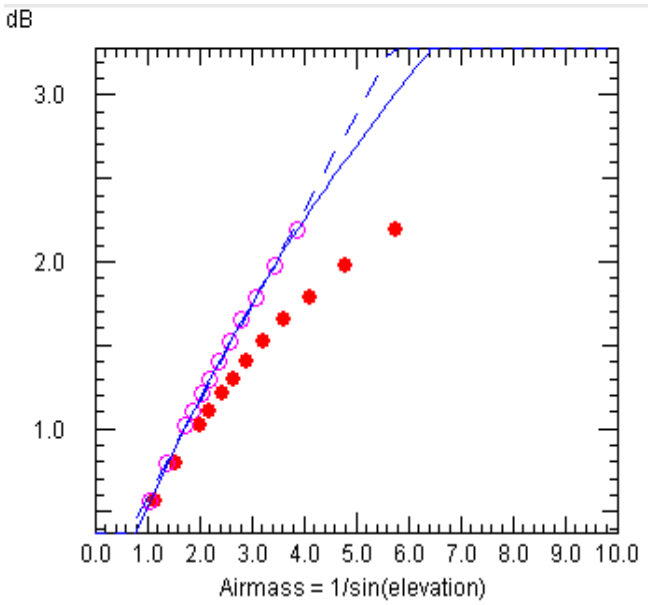

Fig. 13b *with this best value Z the observed powers (red dots) are shifted to the magenta dots through which a straight line (blue) can be well placed. Note that this straight line is distorted due to the use of the dB scale for the ordinate.*

Atmospheric Absorption and the Weather

Quite a few sky profiles have been taken under varying weather conditions. Unfortunately on rainy days, when the sky is full of gray clouds, thermal emission by clouds passing through the field of view causes substantial level changes, so that it is next to impossible to obtain reliable sky profile measurements, as shown in Fig.14, as cloud emission may become as bright as the ground flux calibrator at 290 K!

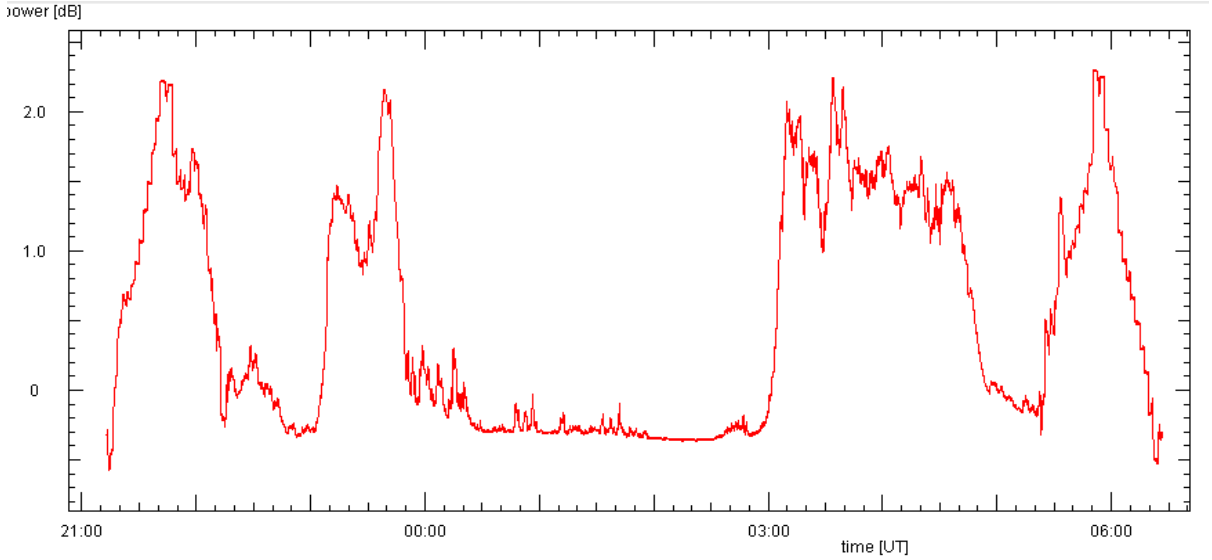

Fig. 14 *Variation of the signal level at 45° elevation during the night of 24/25 july 2015. The sky profile measurements at the start and end of this record are rendered practically useless by the strong thermal emission from passing rain clouds.*

Sky profile data are interpreted by the first method as described in the previous section, but always incorporating the flux calibrator measurement. Depending on the weather, the data vary strongly from undisturbed profiles secured under blue skies (Fig. 11) to profiles disturbed by passing clouds, which nonetheless yield reliable results (Fig. 15).

The table below collects the results from all sky profile measurements.

Date [2015], Time [UT}	T_{sys} [K]	T_{zenith} [K]	sky situation
6 dec 2014 1519	301	30	blue sky
21 may 2118	254	30	blue sky
22 may 1659	221	32	blue sky
24 may 1942	240	23	blue sky
28 may 1700	229	23	blue sky
31 may 1822	255	50	clouds
2 jun 0548	234	40	overcast, light rain
3 jun 1611	232	27	sunny, small clouds
4 jun 2001	237	27	blue sky

Date [2015], Time [UT}		T_{sys} [K]	T_{zenith} [K]	sky situation
6 jun	0808	208	27	overcast
6 jul	1453	189	30	blue sky
6 jul	1913	198	35	blue sky
7 jul	0925	217	56	overcast, drizzle
20 jul	2029	195	41	overcast
20 jul	2105	205	43	overcast
21 jul	0500	177	57	overcast, cloud peaks
21 jul	2058	195	33	blue sky
22 jul	0500	195	37	blue sky, clouds
22 jul	2110	193	36	blue sky, small clouds
23 jul	0500	196	35	light clouds layer
23 jul	2139	192	28	clouds, blue gaps
24 jul	0500	203	32	blue sky
24 jul	2112	182	70	raining
25 jul	0600	171	60	gray overcast, wet
26 jul	0800	204	25	overcast
26 jul	1200	191	30	some white clouds
27 jul	0600	192	43	overcast, cloud peaks
28 jul	0600	197	45	overcast, raining
28 jul	1905	178	45	gray clouds
2 aug	1847	204	35	blue sky, high cirrus
3 aug	1657	180	42	some cirrus clouds
4 aug	0949	200	46	overcast
5 aug	1852	203	35	sunny, light clouds
6 aug	1850	154	52	light clouds

On 8 aug 2015, the horn feed was exchanged. The few results show elevated zenith temperatures despite reasonable weather, which may indicate some not yet identified problems.

Date [2015], Time [UT}		T_{sys} [K]	T_{zenith} [K]	sky situation
10 aug	0440	212	52	overcast
10 aug	1150	231	55	sunny, clouds veil
11 aug	0600	209	52	blue sky, clouds
11 aug	1831	233	46	light overcast

One may draw the following clear conclusions:

- with sunny weather and clear blue skies, the zenith temperature is below about 30 K
- under overcast skies, with dark clouds, and rain, the zenith temperature is substantially higher, 40 to 70 K
- The system temperature is close to 200 K. There is s strong tendency for lower system temperatures to be found at higher zenith temperature, which is obviously due to the interplay of the parameters allowed by the finite accuracy of the fit-by-eye.
  This also demonstrates the difficulties for the derivation of the system temperature that arise when atmospheric absorption cannot be neglected.

In sunny weather (T_{zenith} =30 K, T_{AIR} = 290 K) the zenith attenuation $Z = 4.343 * T_{zenith} / T_{AIR}$ is 0.44 dB, which is quite close to the value of 0.5 dB computed from the ITU Recommendation P.676-10 *Attenuation by atmospheric gases* (Fig.16)

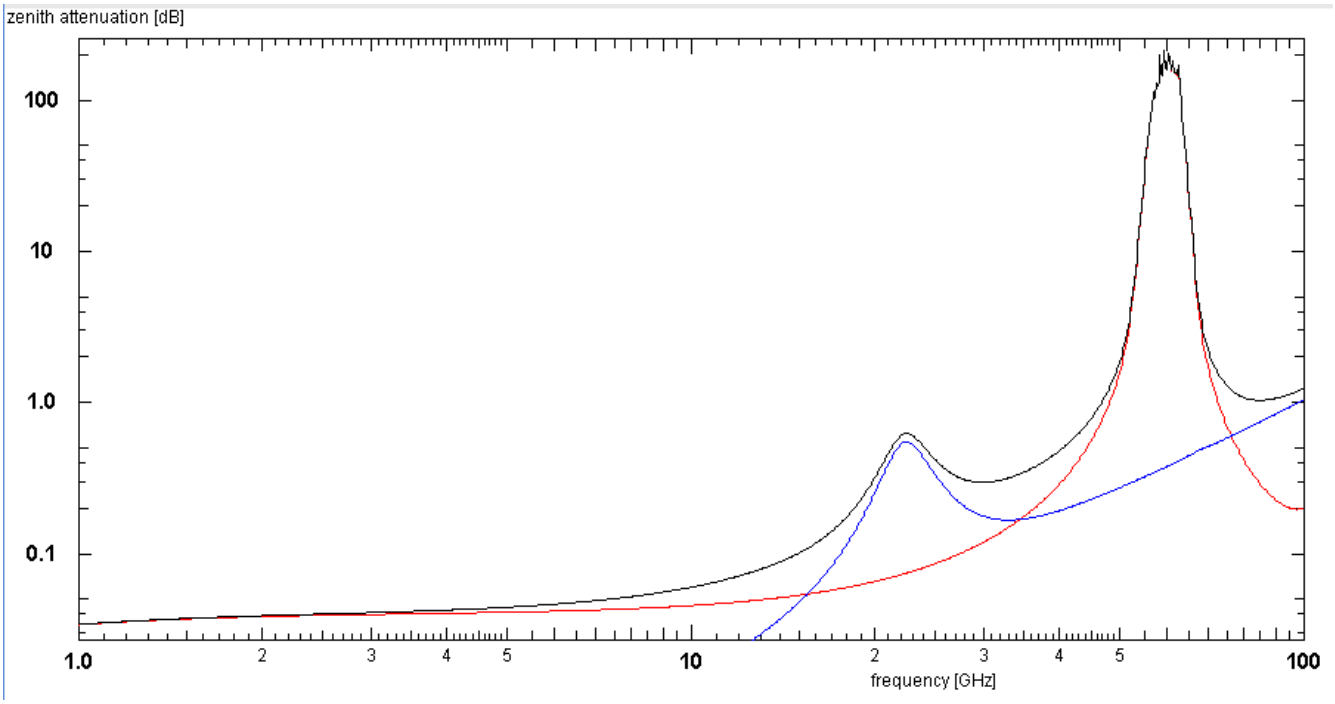

Fig. 16 *Zenith attenuation at sea level for the ITU standard atmosphere (black), dry air (red), and its content of water vapour (blue), computed from ITU Recommendations P.676-10 and P.835-5.*

Solar Flux

Because of the atmospheric absorption the measurement of the radio flux of a celestial body requires the complete procedure of flux calibration and the determination of the sky properties. It is thus of some advantage to follow the Sun on its way to sunset (or from sunrise). Although this takes a couple of hours of observation, one secures a rich amount of data from which a reliable analysis can be performed.
One starts tracking the Sun when it is at elevation of 20° (or higher). At more or less regular intervals the antenna is displaced to the East of the Sun and the sky foreground is measured for a few minutes at the same elevation as the Sun. This is done until sunset.

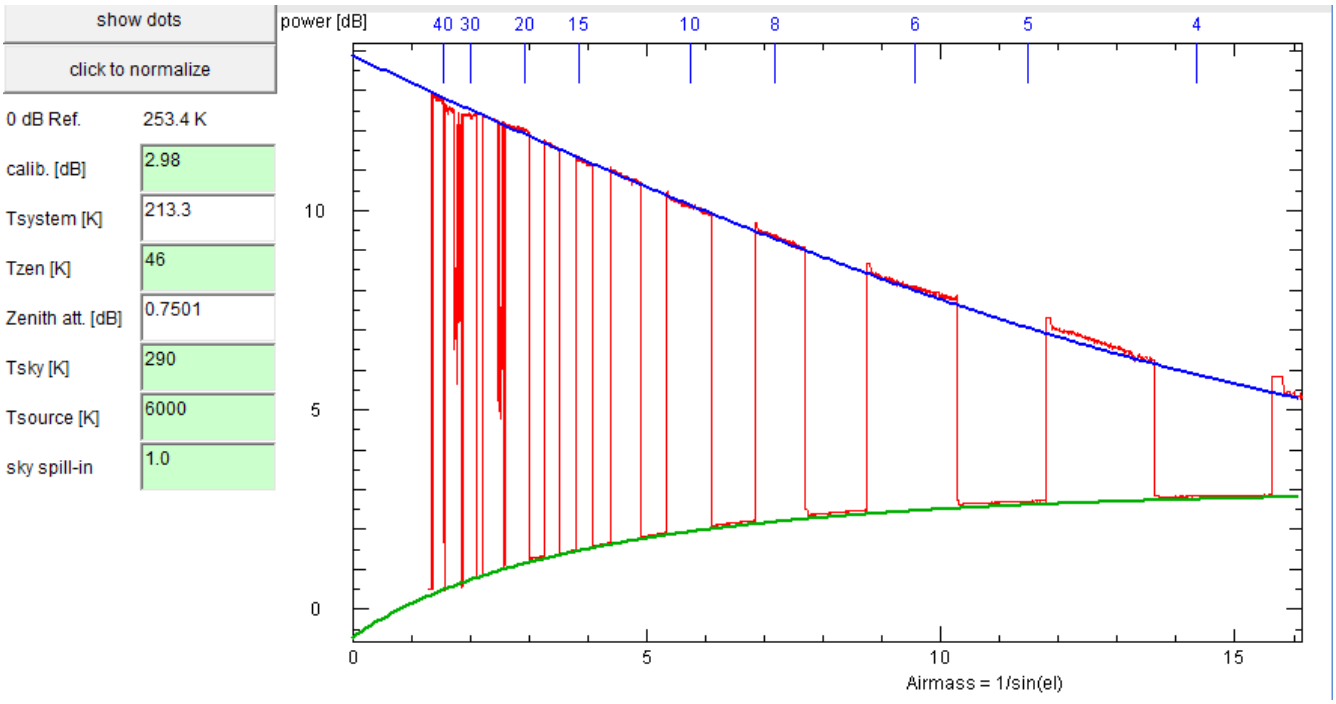

Fig. 17 *Interpretation of data taken by following the Sun until sunset on 11 Aug 2015 (red curve). The green curve is the fit to the measurements for the elevation-dependent sky foreground, taken at position offset East of the Sun, the blue curve is the fit for the solar signal. The blue scale at the top gives the elevations.*

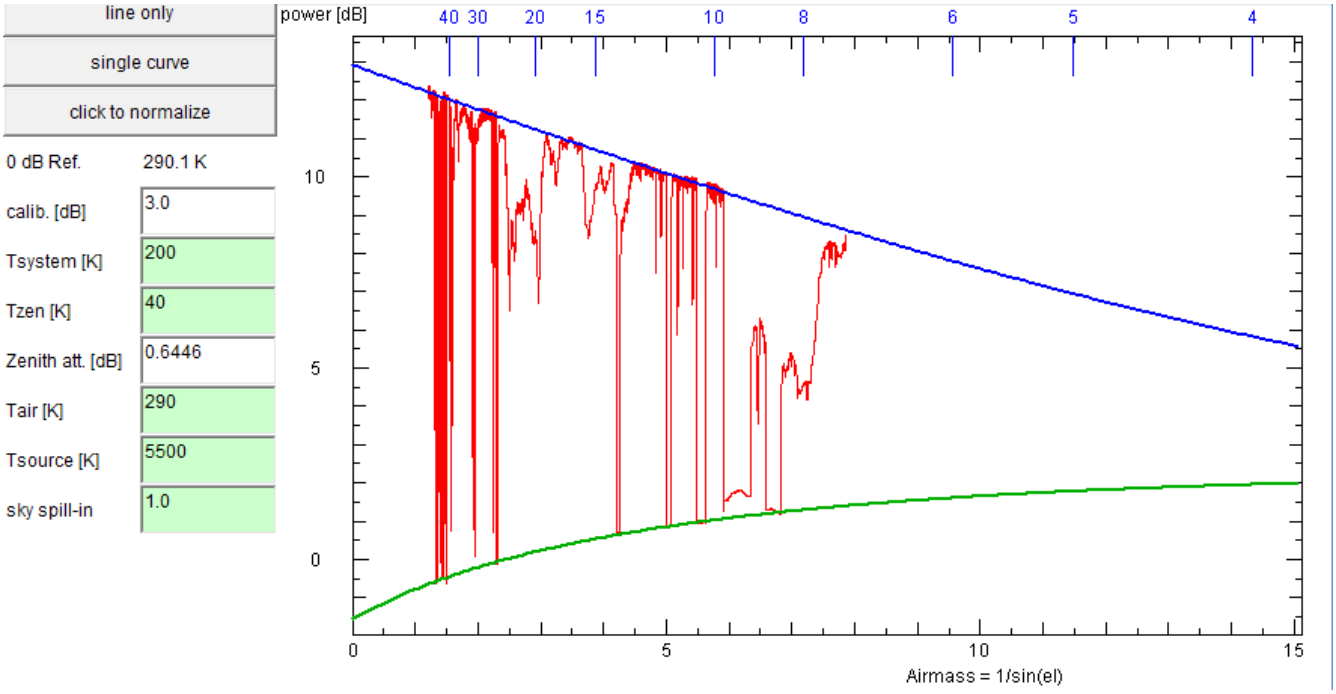

Fig. 18 *Example of sunset observations despite dark clouds and rain (27 jul 2015). Although the sun was tracked only to 8° elevation, and the passing of rain clouds caused strong dips of the solar signal, the data are sufficient to derive a reliable value for the zenith temperature (and absorption).*

As in the analysis of the atmospheric absorption, the measured power is plotted against the air mass, as in Figs.17 and 18. In a first step, the data taken for the sky foreground are matched by adjusting the system and zenith temperatures, which give the green curve. In the above example, the temperature of the air is set to 290 K, so that the zenith absorption is determined by the zenith temperature.
In the second step, the antenna temperature of the source is adjusted as to match the solar measurements with the blue curve which represents the elevation dependence of the attenuation of the solar signal

$$T(A) = T_{source} \exp(-\tau(A))$$

where the optical depth τ is already determined in the first step. It is important to emphasize that the fit of the attenuation of the solar signal represents an independent check of the atmospheric absorption model, which is derived from the atmosphere's thermal emission. Thus, with some further fine-tuning of the parameters a best match of the data by both green and blue curves can be achieved. This procedure also works well, even if the data are perturbed by the absorption and emission from passing dark clouds.

The Table below compiles all sunsets collected so far – interpreted with the assumptions of 200 K for the system temperature and 290 K for the air temperature:

Date 2015	T_{zenith}	T_{source}	sky situation	remarks
29 may	27	5500	overcast, rain	poor data, cloud dips
30 may	22	5900	overcast	cloud dips, imperfect tracking
1 jun	23	5500	blue with small clouds	level changes
3 jun	23	5500	blue with small clouds	level changes
7 jul	45	5500	overcast, drizzle	imperfect tracking
23 jul	27	5700	blue with cirrus clouds	
26 jul	33	6300	overcast	cloud dips
27 jul	40	5500	dark clouds, rain	cloud dips
28 jul	50	6500	dark clouds	chase&measure clouds
4 aug	60	5600	overcast, rain	cloud dips
5 aug	37	6200	light clouds	
6 aug	45	6000	light clouds	T_{sys} = 150K, a shallow dip
10 aug	55	5800	dark clouds, rain	cloud dips
11 aug	46	5800	light overcast	

The correlation between high zenith temperature (thus high atmospheric absorption) found in the skyprofile data is also seen clearly here, with exceptions among the first measurements. In addition, cloudy weather is always accompanied with the presence of dips in the solar signal due to absorbing clouds. On a few days, the sky conditions changed during the observations, indicated by 'level changes'. Due to these changes in the signal level, the interpretation with a signal value for the zenith temperature becomes somewhat difficult. The data from 6 aug are considerably better matched by a 250 K system temperature. There might also be other suitable parameter combinations, which one might be able to find by a stricter search for the best fit …

The antenna temperature is in the range of 5500...6500 K. Due to the finite accuracy of the present fit-by-eye approach, and the interaction of the parameters, one should remain skeptical about the reality of the higher values. With an effective diameter of 1.2 m the effective area is 1.1 m^2, hence the antenna's sensitivity (i.e the ratio of antenna temperature and flux) is

$$T_{ant}/F = A_{eff}/2760 = \ 0.41 \text{ mK/Jy}$$

Hence T_{ant} =5500 K gives a radio flux of 5500/0.00041 = 1.3 MJy = 1342 SFU. This agrees very well with the data from NOAA, which by interpolation yield 1300 SFU at 24 GHz. Note that the flux at this frequency is rather constant, as solar activity does not much affect the flux from the chromosphere.

Interpretation of Antenna Temperatures

To relate antenna temperatures to the physical temperature of a source, the following approximations are usually employed:

- If the source is large enough to fill completely the antenna beam, the source temperature is equal to the antenna temperature
- If the source is smaller than the antenna beam, one corrects for the fraction of the beam which is filled by the source:

  $$T_{source} = T_{ant} / f$$

  with the filling factor f = (source diameter/HPBW)^2

However, when the source angular size is comparable to the HBPW, neither formula works well. The filling factor has to be computed from the antenna pattern and the source intensity distribution.

For the Sun at 24 GHz, one may assume a circular disk of uniform brightness. The antenna is modeled by a uniformly illuminated circular aperture. With these assumptions one gets the results shown in Fig. 19.

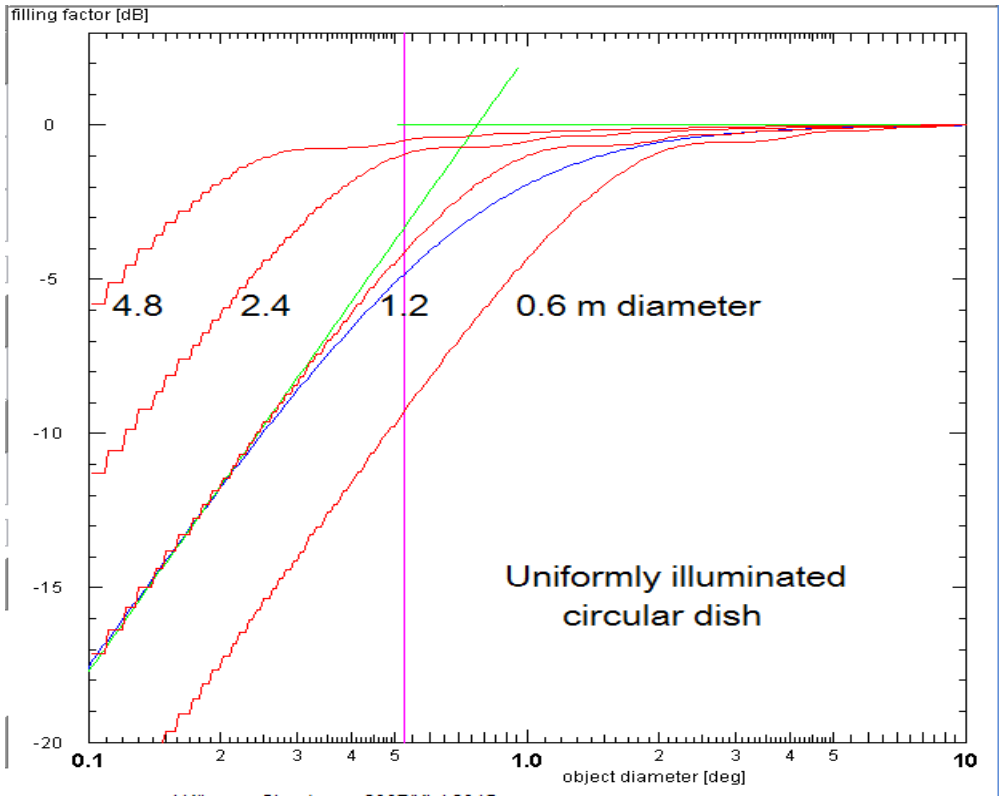

Fig. 19 *Filling factor computed for a solar disk of uniform brightness (angular diameter 0.52°, magenta line) and uniformly illuminated aperture antennas of diameters 0.6..4.8 m for 24 GHz (red curves).The green lines indicate the two approximations, the blue curve is a simple formula to join them.*

For the 24 GHz antenna's effective diameter of 1.2 m, one computes a filling factor of about –4 dB for the Sun. Thus the physical temperature on the solar surface at 24 GHz is

$$T_{sun} = 5500\ K\ *\ 10^{0.4} = 13800\ K$$

which is in agreement with chromospheric temperatures.

Moon Measurements

Several observations of the setting Moon are obtained (Fig. 20). While the interpretation would be similar to that of sunsets, it turns out that because of the much lower contrast against the sky, the derivation of a unique and reliable set of parameters is rather difficult.

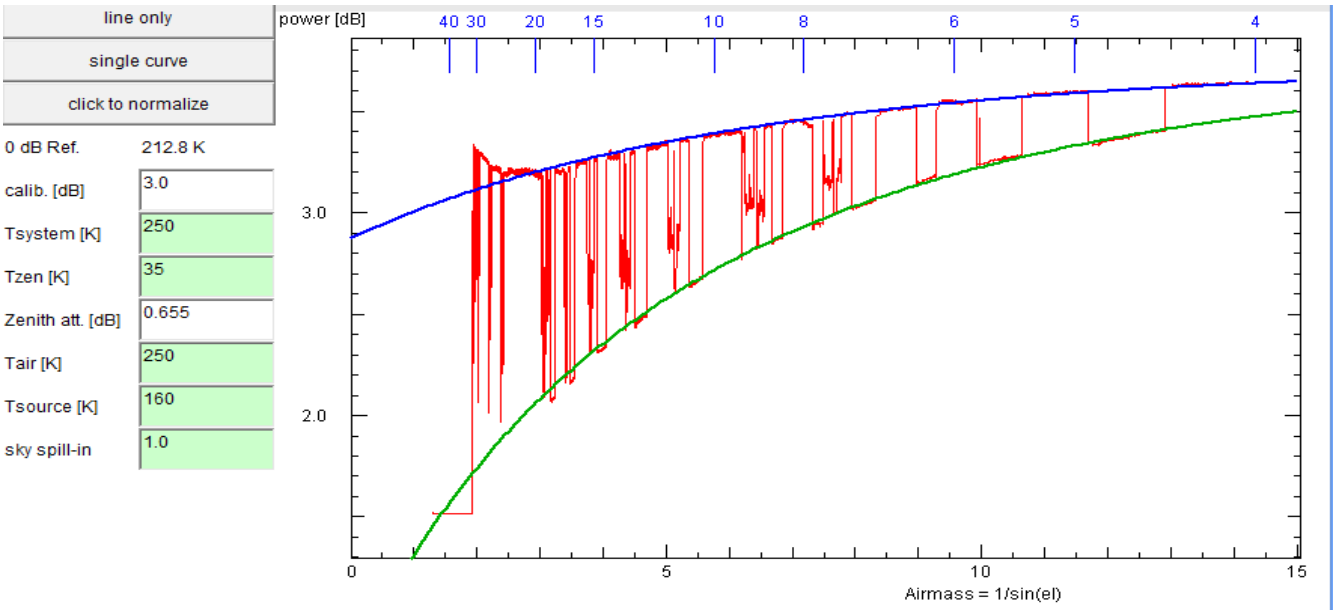

Fig. 20 *One plausible solution of the interpretation of data of the 7 jul 2015 Moon's setting.*

Therefore the results of a drift scan are presented instead: On 5 aug, after two sky profiles complete with flux calibrations, the Moon was observed by a drift scan, albeit at rather low elevation of 10°. Figure 21 shows the raw data.

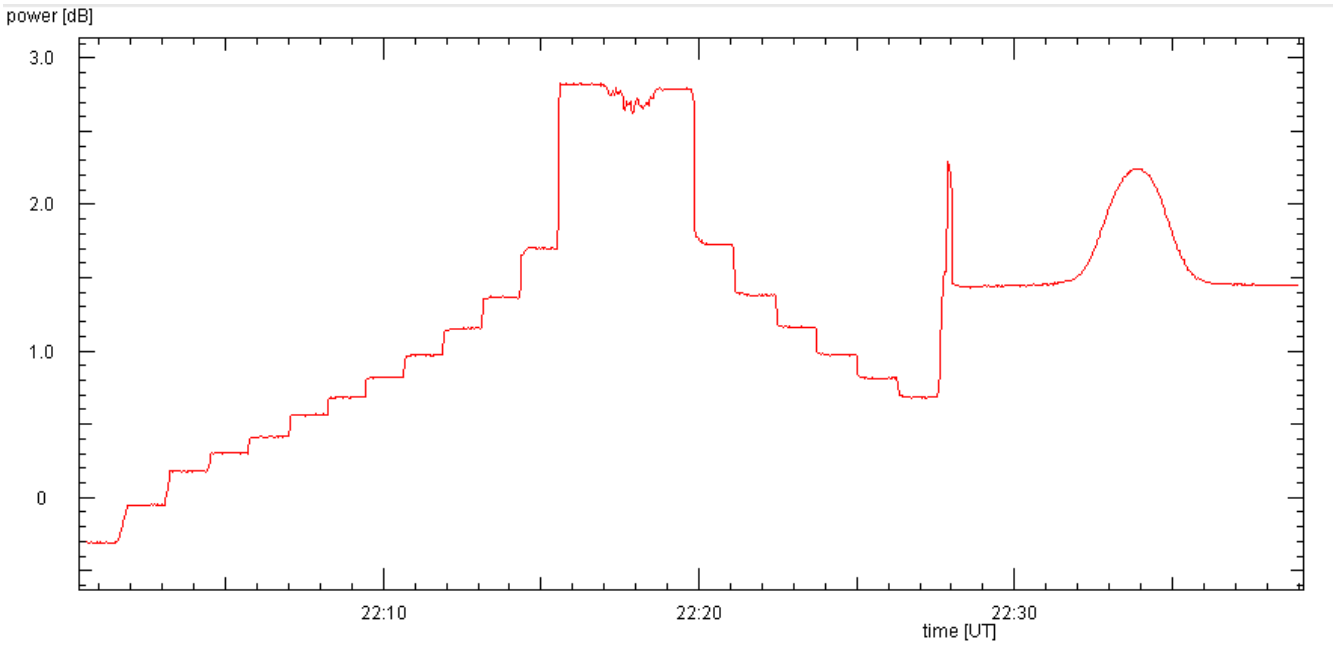

Fig. 21 *Raw data of the Moon drift scan, preceded by sky profiles and flux calibration.*

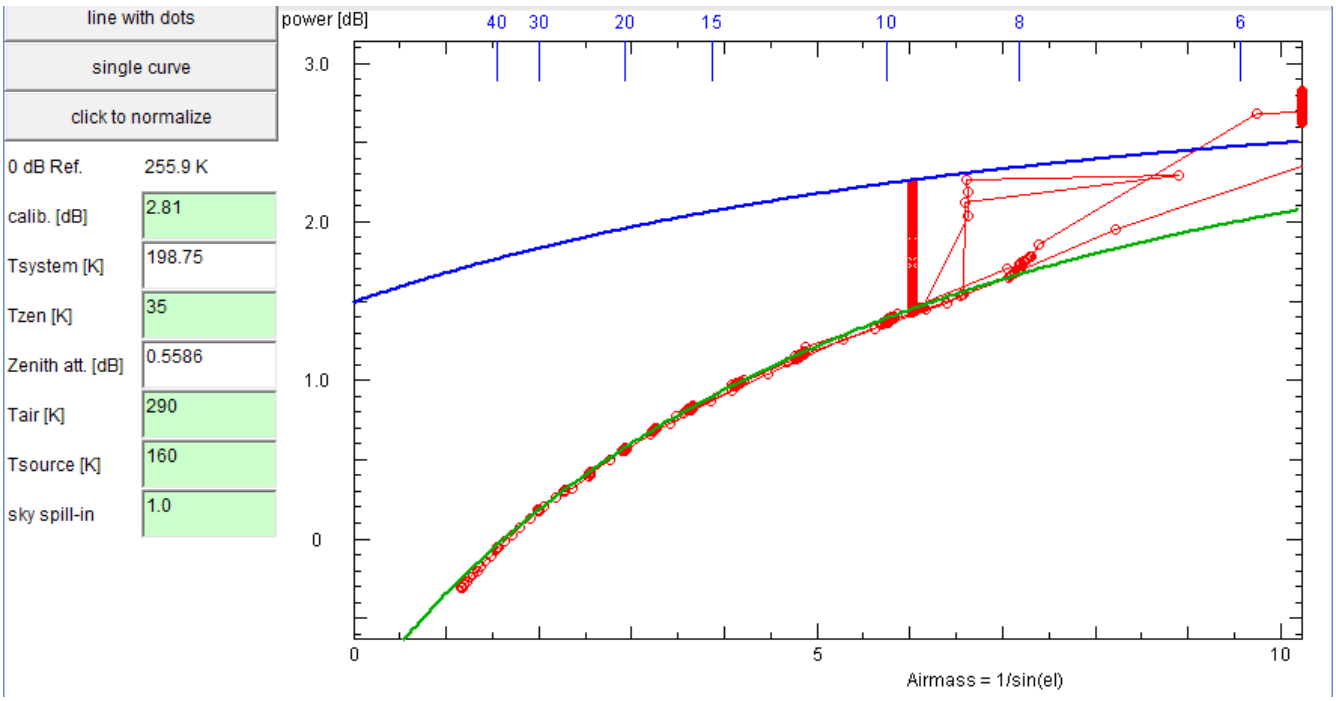

Fig. 22 *Interpretation of the lunar drift scan: the green curve is the fit to the sky profile measurements, based on the flux calibration. The vertical red bar comprises the rise and fall of the signal level during the drift scan at the constant elevation. Thus the blue curve is the model prediction for the maximum of the lunar signal.*

Figure 22 displays the modeling of the measurements by the absorbing atmosphere, whose parameters are well determined due to the flux calibration. One notes that the deduced system temperature is very close to the recommended value of 200 K. From the peak of the lunar signal an antenna temperature of 180 K is derived.

Using, as before, the antenna's sensitivity of 0.41 mK/Jy the radio flux of the Moon is 440 kJy = 44 SFU. This is comparable with the flux of 350 kJy expected from the Moon with a phase-dependent surface temperature.

Temperature of Clouds in the Sky

Dark clouds show up quite prominently on 24 GHz, but in two ways: During their passing between the Sun and the antenna, they reduce the solar radio flux, but when the antenna is pointed at the 'empty sky' thermal emission from the cloud produces an increase of the sky foreground noise.

A period of pretty awful weather can be used to measure the physical temperature of the rain clouds. The theoretical background is the same as had been presented for the absorbing atmosphere:

The radio flux from the Sun is reduced by the absorption of a cloud of optical thickness τ

$$T = T_0 \exp(-\tau)$$

where T_0 is the antenna temperature of the unobscured Sun. This cloud also emits thermal radiation whose strength depends on its temperature T_{cloud} and its optical thickness: The antenna temperature is

$$T = T_{cloud} (1 - \exp(-\tau))$$

This formula has two limiting cases: The emission of a rather transparent cloud ('optically thin' $\tau << 1$) increases with its optical thickness

$$T = T_{cloud} (1 - \exp(-\tau)) \approx T_{cloud} (1 - (1-\tau)) = T_{cloud} * \tau$$

but an opaque viz. optically thick cloud ($\tau >> 1$) emits radiation corresponding only to its physical temperature:

$$T = T_{cloud}$$

since $\exp(-x) \rightarrow 0$ for large x.

This means that a more transparent cloud reduces the solar signal by a small amount and emits also only a weak signal. An opaque cloud will strongly block the sun, but is also visible as a bright source in the sky. One may take $\tau = 1$ as a rough border between the optically thin and thick regimes. This corresponds to an attenuation of the solar signal by $10*\log_{10}(\exp(1)) = 4.343$ dB.

While tracking the Sun, one waits until its signal is strongly reduced. Then one points the antenna away to pick up the emission of the obscuring cloud (if it is large enough). This is shown in Fig.23.

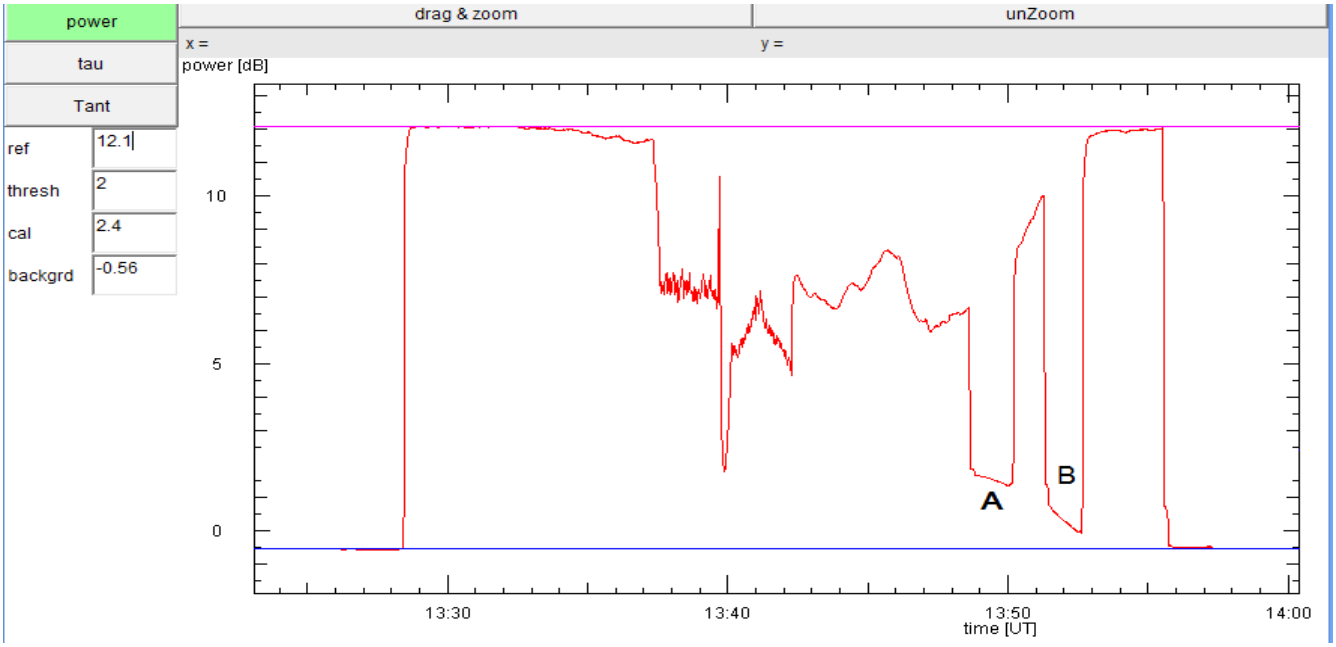

Fig. 23 *Raw data of observations of rain clouds: The horizontal magenta line marks the level of the signal of the unobscured Sun, the blue line denotes the assumed level of the 'normal sky'. At two instances, A and B, the antenna is pointed away from the Sun, to pick up the cloud's thermal emission.*

At UT 12:38 a measurement of the Sun's position was attempted, despite a slight decrease of the solar signal. As the signal level changed more strongly, this attempt was abandoned at UT 12:42. Since the solar signal drops by more than 4.3 dB below its normal level, the clouds in the sky have become optically thick. At two instances, A and B, the antenna is pointed about 5° East of the Sun, and thermal emission from the sky is measured.

Since the ratio (i.e. the difference in dB) of the actual solar signal p_{dB} and the unobscured level p_0 allows to measure the optical thickness at any moment

$$\tau = (p_0 - p_{dB}) / 4.343$$

the variations of the solar signal yield the time variation of the optical thickness. This variation is interpolated for the times when the antenna was turned away from the sun. Figure 24 shows that at two moments the optical thickness exceeds 1.

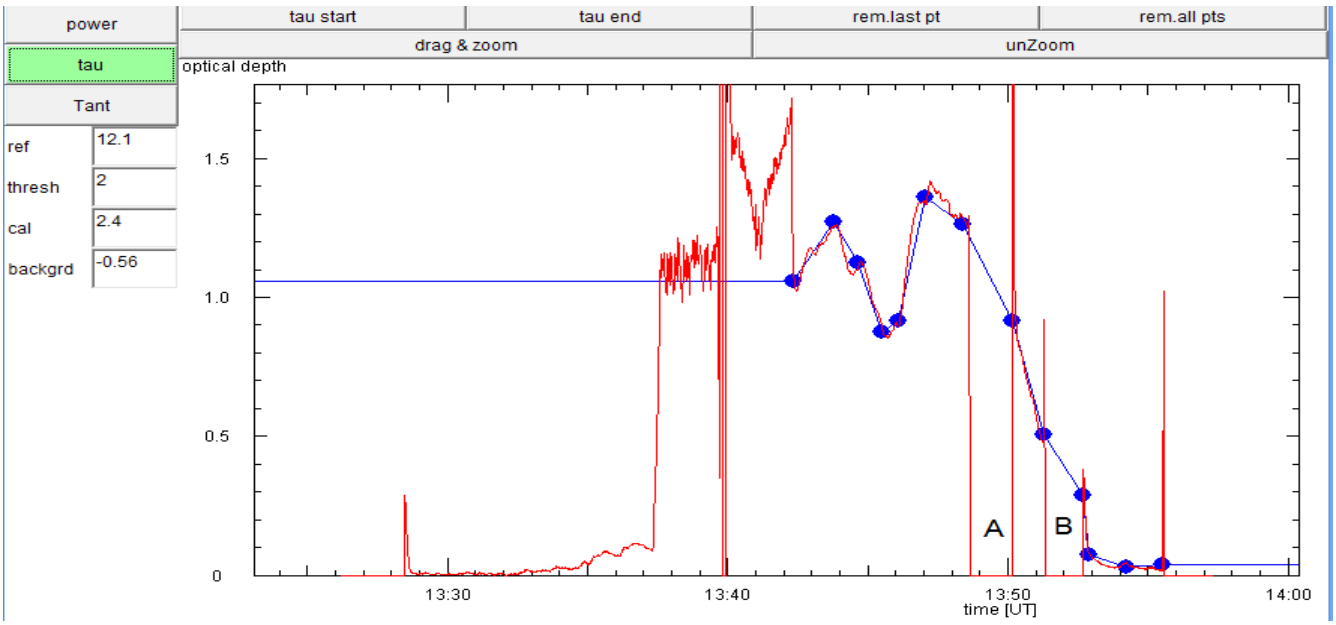

Fig. 24 *Manual interpolation (blue curve) of the time variation of the optical thickness of the cloud cover.*

The blue curve allows to interpolate the optical thickness at all times. On may then deduce the physical temperature of the clouds during the intervals A and B, when the emission is measured:

$$T_{cloud} = T/(1 - \exp(-\tau))$$

This is done in Fig.25. It shows that the temperature at A and B was nearly constant, and close to 300 K – as one would have surmised.

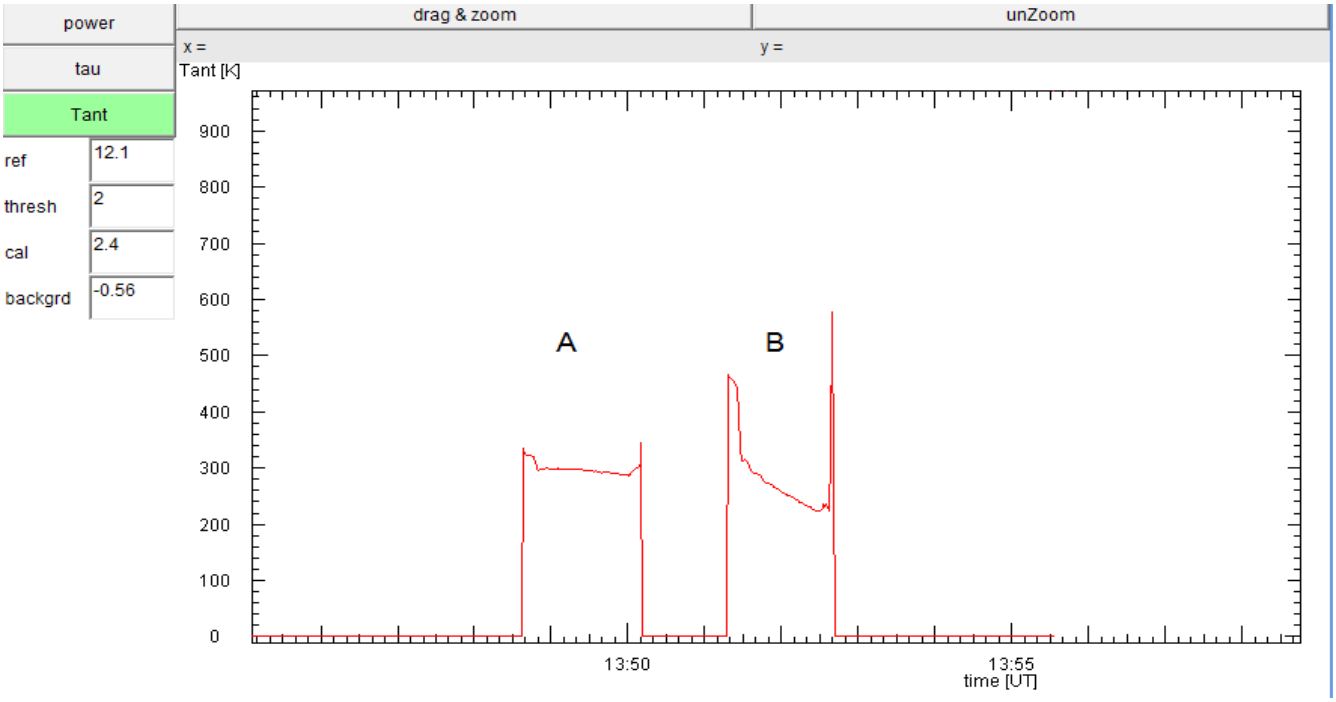

Fig. 25 *The deduced physical temperatures of the clouds A and B.*

Conclusions

The state of the 24 GHz antenna can be described as follows

- with the improved pointing correction model, the instrument can track the Moon and the Sun on their entire path across the sky, with a residual error of a few 0.01°
- the present feed illuminates only 10 percent of the reflector's surface. The HPBW is about 0.6°, and the antenna gain about 49.6 dBi, the effective area is 1.1 m^2
- the system temperature is close to 200 K
- the absorption of the atmosphere is measured reliably by sunsets and sky profiles. The zenith temperature is found to vary from 25 K for a blue sky to 70 K under rain clouds. These values correspond to zenith attenuation from 0.37 to 1.1 dB, which agrees well with ITU Recommendation P.676-10
- solar radio flux can be measured by observing sunsets (and sunrises) which allow correction for the atmospheric absorption. The derived flux agrees well with NOAA measurements
- lunar radio fluxes can be measured, but the correction for atmospheric absorption is more difficult at these lower signal levels
- the physical temperature of rain clouds can be determined, and is near 300 K
- atmospheric absorption makes the interpretation and the derivation of system temperature much more difficult. The presently used method of observation and analysis needs further improvements

References

ITU-R Recommendations for Radio Propagation:

- Reference standard atmosphere: http://www.itu.int/rec/R-REC-P.835/en
- Attenuation by atmospheric gases: http://www.itu.int/rec/R-REC-P.676/en

DL0SHF Technical Notes

- Measurements at the DL0SHF 1 GHz radio telescope
  http://sat-sh.lernnetz.de/pdf/DL0SHF_1GHz.pdf
- Pointing correction for the DL0SHF 24 GHz antenna
  http://sat-sh.lernnetz.de/pdf/PointingCorrection24GHz.pdf
- Pointing correction at DL0SHF 10 GHz
  http://sat-sh.lernnetz.de/pdf/Pointing10GHzTwo.pdf